TALLINNA TEHNIKAÜLIKOOL
TALLINN UNIVERSITY OF TECHNOLOGY

SCHOOL OF ENGINEERING

DEPARTMENT OF MATERIALS AND ENVIRONMENTAL TECHNOLOGY

LABORATORY OF POLYMERS AND TEXTILE TECHNOLOGY

"SHRINKAGE AND WARPAGE REDUCTION OF FILLED AND BLENDED POLYPROPYLENE FOR EXTRUSION-BASED ADDITIVE MANUFACTURING"

Master Thesis of

Chethan Savandaiah

Supervisor: Prof. Dr. Holzer Clemens

Head of Polymer Processing,

Montanuniversitaet, Leoben.

Co-Supervisor: Prof. Dr. Krumme Andres

Head of the Laboratory

Tallinn University of Technology

Technology of Wood and Plastic, KVEM 12/13

Tallinn, 2017

TALLINNA TEHNIKAÜLIKOOL
TALLINN UNIVERSITY OF TECHNOLOGY

INSENERITEADUSKOND

MATERJALI- JA KESKKONNNA TEHNOLOOGIA INSTITUUT

POLÜMEERIDE JA TEKSTIILI TEHNOLOOGIA LABOR

“Kahanemise vähendamise uurimine Polypropüleeni kompaundides ekstrusioon-tootmisel saadavates segudes”

Magistritöö

Chethan Savandaiah

Juhendaja: Prof. Dr. Holzer Clemens

õppetooli juhataja, Polümeeride töötlemine,

Montanuniversitaet, Leoben.

kaasjuhendaja: Prof. Dr. Krumme Andres

Labori Juhataja

Tallinn University of Technology

Puidu- ja plastitehnoloogia, KVEM 12/13

Tallinn, 2017

Declaration

Hereby I declare that this master thesis, my original investigation and achievement, submitted for the master degree at Tallinn University of Technology has not been submitted for any degree or examination.

Chethan Savandaiah

Acknowledgement

I would like to express my gratitude to my supervisor Univ. Prof. Mag. Dr. Clemens Holzer, head of the Chair of Polymer Processing at the Montanuniversitaet Leoben, for the enablement and the final assessment of this master thesis. I am grateful for the opportunity I have been given to do an internship and pursue my master thesis in Leoben.

I would like to express my sincerest thanks to Mrs. Suld Tiia Maaja, Specialist, Tallinn university of technology, Tallinn for introducing me to this wonderful traineeship opportunity and guiding me all along the length of my training. I would like to express my sincerest thanks to Prof. Dr. Krumme Andres, Head of the Laboratory of Polymers and Textile Technology.

But first and foremost, I offer my special gratitude to my mentor Dipl.-Ing. Spörk Martin, who stood by my side in every imaginable situation with his very composed and easy-going character. Without his helpful guidance at the beginning of the practical part of this work, and also without his continuous assistance, both during the lab operations and the corrections of the written work, I would have spent far more time on this project. Without his help, this work could have never have been finished on time. I am also very grateful to Dipl.-Ing. Schuschnigg Stephan for his assistance in reviewing and continuous input regarding correction of my thesis work and his willingness to help me in any situation. Gratitude is also owed to Dr. Janak Sapkota for his timely guidance and guiding me in scientific direction in analysing the results. I would like express my gratitude to the rheology lab staff Sabrina Winkler and Julia Gössmann, who always helped me in daily lab activities.

Additionally, I wish to thank my colleagues at the chair of polymer processing, Montanuniversitaet Leoben, especially the extrusion group and Laboratory of Polymers and Textile Technology, Tallinn University of technology, Tallinn, and my fellow students for their useful advice in the lab and with this work.

Last, but not least, my family and friends who have constantly pushed me to achieve accomplishment and held my hands and guided me during difficult time, I express my sincerest thank you.

I would also to like acknowledge European Union and ERASMUS + SMP for providing me with needs and necessity, and also the ERASMUS office at both universities for their helpful guidance.

Abstract

Polypropylene (PP) is semi crystalline in nature and therefore undergoes shrinkage. Using unfilled PP as a filament for FFF is not viable due to its dimensional instability occurring during and after printing of the product. In order to achieve printable parts, it is crucial to reduce the material's tendency to warp, as well as to improve the filament's mechanical and flow properties, and its elasticity. Thus, it is essential to fill and blend PP with spherical fillers and amorphous materials. In this work the main focus lies on the formation of PP compounds consisting of two types of spherical solid glass beads in different sizes. The addition of 30 vol.-% of fillers, independent to the filler size, showed a strong reduction in the material's shrinkage, without changing the degree of crystallinity of the compounds. The inorganic boro-silicate glass type revealed far better mechanical properties, as well as a drastic increase in crystallization temperature, a more even filler distribution and a better compatibility to the polymer, compared to the inorganic soda lime glass. The mechanical properties of the most promising compounds were optimized for 3D printing by means of melt blending with three different amorphous polymers. Best results were achieved with amorphous polyolefin, which compound was possible to extrude in a good quality in a big scale. The printing of this compound revealed a drastic improvement in warpage compared to unfilled PP.

Abstrakt

Polüpropüleen on oma olemuselt poolkristalliline polümeer mistõttu kõvenemisel ilmneb produktidel dimensionaalne kahanemine, mis teeb polüpropüleeni kiu kasutamise 3D printimisel (FFF-s) sobimatuks. Printimiseks sobiva materjali saamiseks on vaja vähendada kahanemist kõvenemisel ja samaaegselt parandada filamendi mehaanilisi näitajaid, voolavust ja elastsust. Seega on otstarbekas kasutada polüpropüleeni kompaundi saamisel sfäärilist või amorfset materjali. Filamendina kasutatakse polypropüleeni kompaundi.

Antud töös on kasutatud polüpropüleeni kompaundide saamisel kahte tüüpi erineva suurusega tahkeid sfäärilisi klaaskuulikesi. 30% täitaine lisamisel ilmneb kahanemise vähenemine ja kristallilisuse astme suurenemine kompaundis. Anorgaanilise boro-silikaat klaasi kasutamine mõjutab enam mehaanilisi omadusi , muutmata kristallumise temperatuuri, paremat täiteaine jaotust ja sobivust polümeeriga võrreldes anorgaaliliste lubi-klaasi kuulikeste kasutamisega. Enam sobivate mehaaniliste omadustega kompaundid optimeeriti kolme erineva amorfse polümeeriga ekstrusioon meetodil 3D printimiseks sobivaks filamendiks, kus suures mastaabis ekstrudeerimiseks osutus sobivaimaks polüolefiinne kompaund. Printimisel selgus drastiline kahanemise vähenemine võrreldes täiteaineta polüpropüleeni kasutamisega.

Table of Content

1 Introduction and Objectives

The main aim of this research work was to control and optimize the dimensional stability and warpage of polypropylene (PP) in extrusion based additive manufacturing. In order to achieve printable filament it is essential to improve the filament's mechanical and flow properties, as well as its elasticity. Extrusion based additive manufacturing, also known as fused filament fabrication (FFF), was developed in the 1980's. Recently this technique gained popularity due to the fact that most of the intellectual properties of the technology expired. Moreover with improvement in the quality of the printed products it has become evident to compare it with the products produced from conventional technique such as injection molding.

So far, a lot of research that deals with making additive manufacturing user friendlier has been published. However, only little progress has been made on the development of new materials. With only few commercial available materials, such as PLA (polylactic acid), ABS (Acrylonitrile butadiene styrene), and ABS-PC (Acrylonitrile butadiene styrene-polycarbonate), the extrusion-based additive manufacturing technique has only found limited application in the industry.

That is why now is the time to develop new materials for FFF in order to broaden the area to commodities products, as well as for complex structural applications. In principle, we can further enhance extrusion-based additive manufacturing by developing novel materials.

One of the potential polymers to focus future research on is PP. Due to its inherent nature of semi-crystallinity [46], it exhibits excellent material properties, such as high stiffness, good modifiability [7, 9, 46, 57], high mechanical strength [46], well-known processing conditions, excellent resistance to hydrolysis [46], and moisture absorption. PP would be an ideal and unique material for FFF.

However, the foremost issue of using unfilled PP as a filament for FFF is its dimensional instability occurring during and after fabrication of the product. Due to its high degree of crystallinity, non-isotropic shrinkage along and across the flow directions occurs [15, 38, 46, 76]. As a result this high shrinkage coefficient [38] limits the application of PP in FFF as the printed parts warp easily. Therefore, for most polyolefins not even the first layer of printing can be produced, because their high degree of warpage hinders the other layers to be printed. However, due to PP's excellent modifiability, its properties can partly be fine-tuned to the requirements for specific applications.

In this thesis, the main focus was to optimize the non-uniform shrinkage and warpage of neat PP by incorporating fillers such as glass beads and blending rubbery materials such as thermoplastic elastomers (TPE), amorphous polyamides (am.PA), and amorphous polyolefins (am.PO).

The main interest for using glass beads as a filler material is due to its low aspect ratio which results in isotropic and uniform shrinkage. Polymers containing fillers such as fibers cause anisotropic shrinkage and warpage [49] leading to dimensional variation during molding or production.

Moreover, incorporating fillers in PP may increase certain mechanical properties, such as stiffness and tensile strength, but may also reduce the required processing properties and its elasticity. Neat PP, for example is tough, can undergo deformation without breaking, but it might undergo physical changes once it is incorporated with fillers. Such a change could result in processing difficulties. Thus, it is necessary to blend the PP compounds with rubber like materials to retain certain processing properties.

The research work carried out was mainly focused on the influence of the filler size, filler type and filler loading, with and without silane coating, on the shrinkage of PP. Furthermore, the effects of blending the compounds with amorphous-like materials on the processability, as well as its mechanical properties were studied.

The fundamental knowledge gained during this research will open up new frontiers for material development adding more potential to the catalogue of materials available for 3D printing. In addition, it has the possibility to create efficient processing parameters for the application in the industry.

2 Theoretical background

2.1 Extrusion-based additive manufacturing

For the past two decades the rapid prototyping technology has developed rapidly, but the principles of the technology remain more or less unchanged. The fabrication of flexible and complex geometric design, its cost efficiency, and processability have made rapid prototyping a lucrative business opportunity.

The first extrusion-based additive manufacturing technique was called Fused Deposition Modeling (FDM), developed and patented by Stratasys in 1991. Another name of this technique is Fused Filament Fabrication (FFF), which will be used throughout that work, as FDM and "Fused Deposition Modeling" are trademarks of Stratasys. The basic principle of FFF is that a thermoplastic filament is fed into a moving nozzle through two counter-rotating driving wheels. The nozzle is heated above the melting temperature of the material and the melt is deposited on a hot printing bed [18, 21]. The material deposition is based on a layer by layer method, generating objects on the base of CAD drawings (see Figure 1) [21].

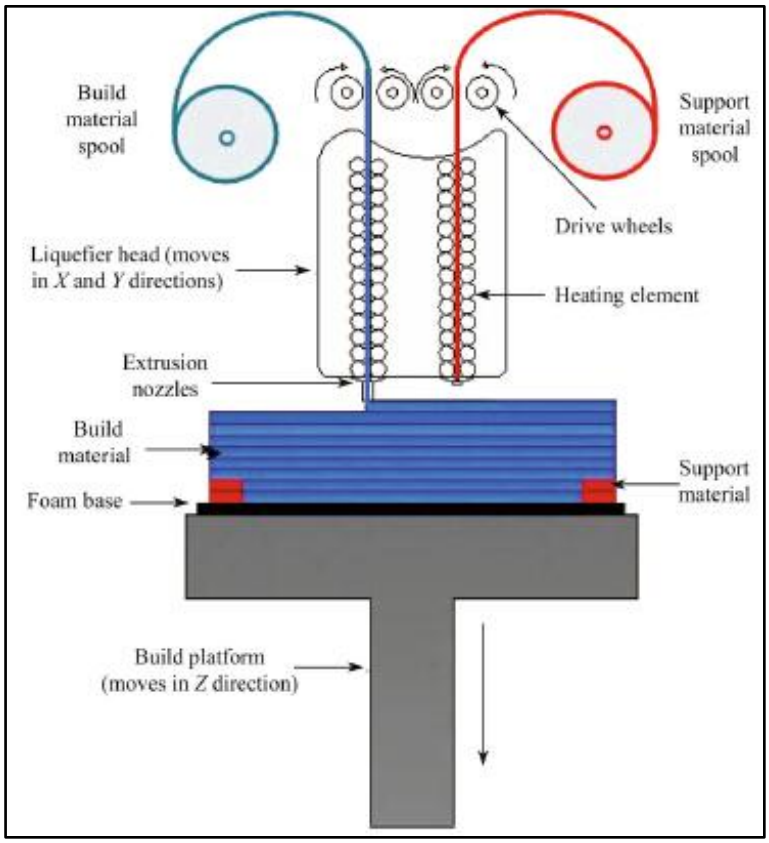

Figure 1: FFF typical equipment setup [45].

The processed thermoplastic material cools down below its melting temperature, but above glass transition temperature thereby seizing the still moving polymer chains into the adjacent strands. The cohesion property between the deposited melt is highly dependent on the interfusion of the polymer chains at the interface [18, 21], i.e., between melt and solidified layer. In order to achieve better cohesion between the deposited layers it is essential to heat the bed above the glass transition temperature of the printing material.

The nozzle diameter and the resulting diameter of the extruded material defines the minimum layer thickness [18, 21, 45] ranging from 0.1 mm to 0.5 mm. Thus, the maximum achievable resolution of the printed parts is approximately 100 µm.

Compared to other additive manufacturing techniques, the FFF technology enables to produce relatively large volume in a short period of time with a huge variety of thermoplasts. However, like all processing techniques, also FFF has its disadvantages. For example, due to its limiting spatial resolution of 100 µm the printed parts obtain a rough surface quality. Only with proper post-processing techniques this shortcoming can be improved.

An FFF process usually starts with a CAD file in a .stl format, outlining the design elements. The description of the object is based on triangles describing the surfaces of the object. A special software called slicer creates profile sections over the height of the object. It defines the infill of each part and sets the plotting area and path for the nozzle. As a result, the slicing software creates the opportunity for effective deposition of material for ideal product conditions [18, 21, 45].

2.2 Polypropylene

PP gained commercial prominence during the 1960's due to the breakthrough of synthesizing PP in huge amounts, resulting in being currently one of the major commodity plastics [46]. In general PP exhibits optimal mechanical properties, such as elevated tensile strength, good impact behaviour and a high resistance to fatigue. Moreover, the substitution of one hydrogen group with a methyl group on every second carbon (see Figure 2) gives unique property features compared to polyethylene such as higher stiffness and a much better abrasion resistance [23]. In addition, PP is one of the lightest plastics [23] with a density of 0.905 g/cm^3.

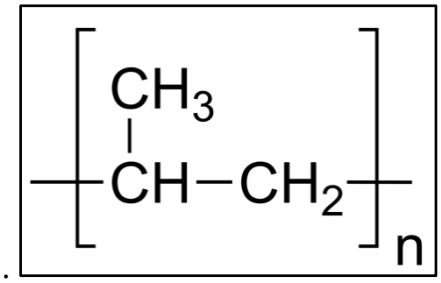

Figure 2: Chemical structure of PP [23].

The presence of the methyl group enables the formation of stereoregularity, which means that the methyl group can be arranged differently on the backbone of the main chain (see Figure 3). If the methyl group is attached to the tertiary carbon on the same side, the formation is called isotactic PP. If it is attached alternatively from one side to another, it is called syndiotactic PP. Both of these isomers result in very semi-crystalline material due to their easy arrangement in regular segments. The synthesis of syndiotactic PP was first reported by Natta and his coworkers in 1960-62, which was a real break-through for the polymer industry [46, 65, 74]. Before Natta et al., the only PP that could be synthesized was the atactic form, in which the methyl groups are randomly attached to tertiary carbon. This isomer results in very poor mechanical properties and behaves similarly to a wax. The rigid and strong nature of isotactic and syndiotactic PP is due to its ability to pack bulky macromolecules tightly into a crystalline structure. On the contrary, the rubbery nature of atactic PP originates from the bulky methyl group which hinders tight packing to form crystalline regions.

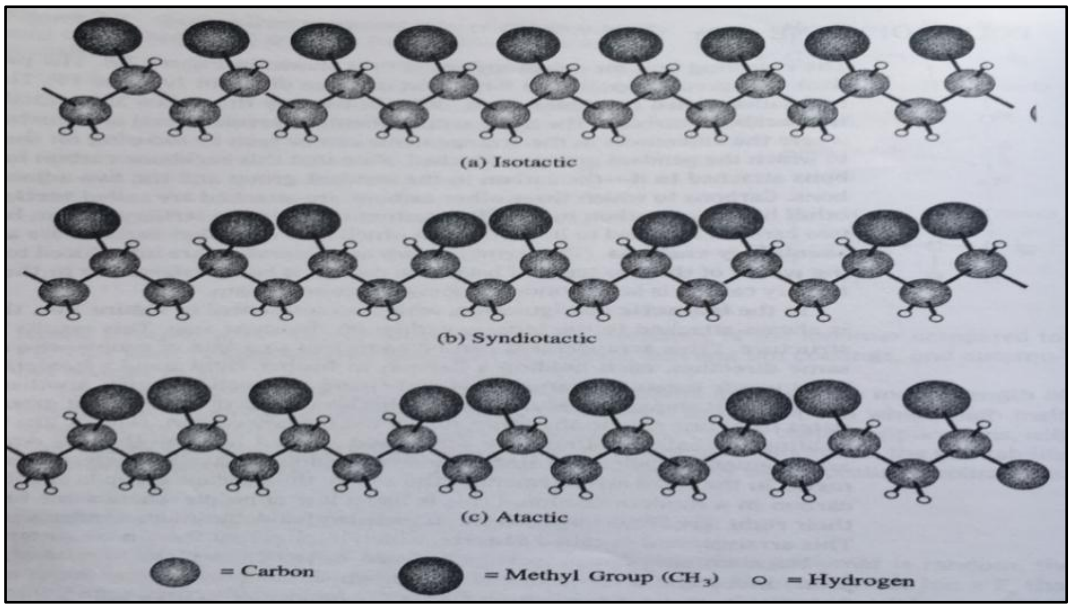

Figure 3: Stereoisomerism of polypropylene [65].

The PP's superior stiffness, its low density and its low cost make PP together with the easy possibility to add fillers an ideal material for the usage as engineering plastics in structural applications [57, 65]. Having a glass transition temperature of -20 to 0 °C, depending on the spatial arrangement of the methyl groups, PP provides good stability from 0 to 150 °C. However, at low temperature (below 0 °C) isotactic and syndiotactic PP is brittle, which can be improved through co-polymerization with polyethylene or diene monomers. Since PP is a semi-crystalline polymer, its service temperature usage is limited by its melting point at 165 °C [23, 46, 57, 65].

2.3 Shrinkage

The intrinsic cause of shrinkage of polymers is based on the thermodynamic behaviour of the material [3]. Most semi-crystalline polymers, like PP, shrink six times more than amorphous polymers [15]. In their relaxed state, the polymer chains of semi-crystalline polymers are structurally arranged or aligned, whereas the macromolecules for amorphous polymers are completely random oriented. During melting of semi-crystalline materials, the crystalline structures disappear and the chains move randomly. When semi-crystalline polymers are cooled down below their crystallization temperature, the chains tend to orient themselves to form ordered structures again. They never form full crystals, but islands of crystals surrounded by amorphous material (see Figure 4) [15]. Crystalline polymer chains have to realign considerably to achieve their order and packing for a relaxed state. Amorphous polymers, on the other hand, inherently have random chain orientation and require less realignment to reach their relaxed state during cooling. As a result, semi-crystalline polymers shrink considerably more in an anisotropic manner at various positions. Thereby, leading to different amount of shrinkage in the flow direction and in the transverse flow direction, which results in warpage [3, 15, 23, 46, 57, 74]. A slow rate of crystallization or a low degree of total crystallinity reduces the shrinkage and therefore also the warpage. The crystallization continues below the melting point and above the glass transition temperature. As a result, the more the material crystallizes, the more it shrinks [3].

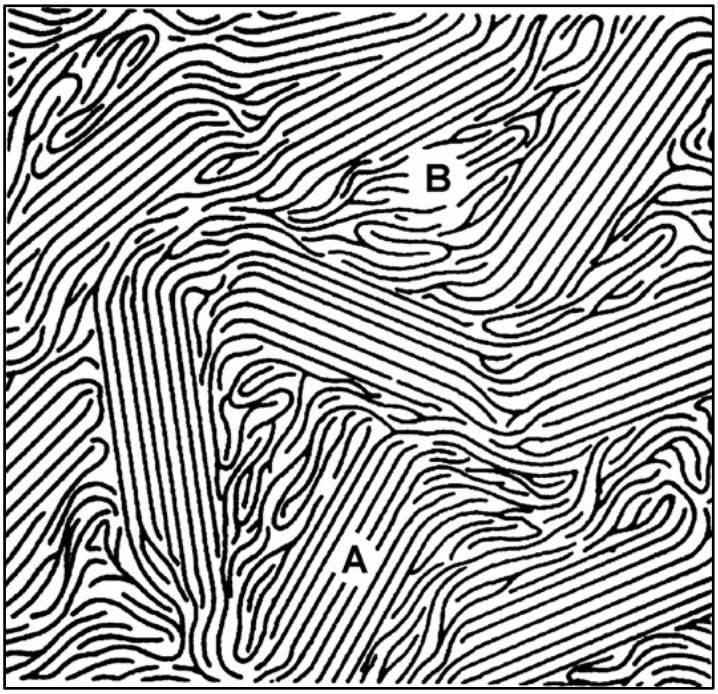

Figure 4: An illustration of a semi-crystalline polymer at room temperature. Area ‘A’ represents the crystalline area, and ‘B’ represents the amorphous area [9].

2.3.1 Method to determine the shrinkage of polymers

Material properties, such as the dependency in pressure, specific volume and temperature, as well as the morphology and the crystallinity of the material are major factors influencing the shrinkage behaviour. One of the reliable methods to measure shrinkage is the pvT measurement. The specific volume of the material is measured as a function of both the temperature T and the pressure p, as described by its pressure-volume-temperature (pvT) relationship. It is possible to investigate the complete phase behaviour of a material by means of pvT, for example the melting of a polymer [3, 8, 15].

In Figure 5 the pvT-diagrams for an amorphous, as well as a semi-crystalline material is depicted. In melt condition, both semi-crystalline and amorphous material show linear dependency of the specific volume on the temperature. For the solid phase, a considerable difference can be noted due to crystallization in semi-crystalline material. The specific volume decreases exponentially with decreasing temperature for semi-crystalline materials (see Figure 5b), whereas only a slight decrease can be noted in amorphous materials (see Figure 5a). The change in specific volume can be related to the shrinkage of the material.

Hence, pvT is an ideal measurement to characterize the material's shrinkage during cooling [3, 8, 57].

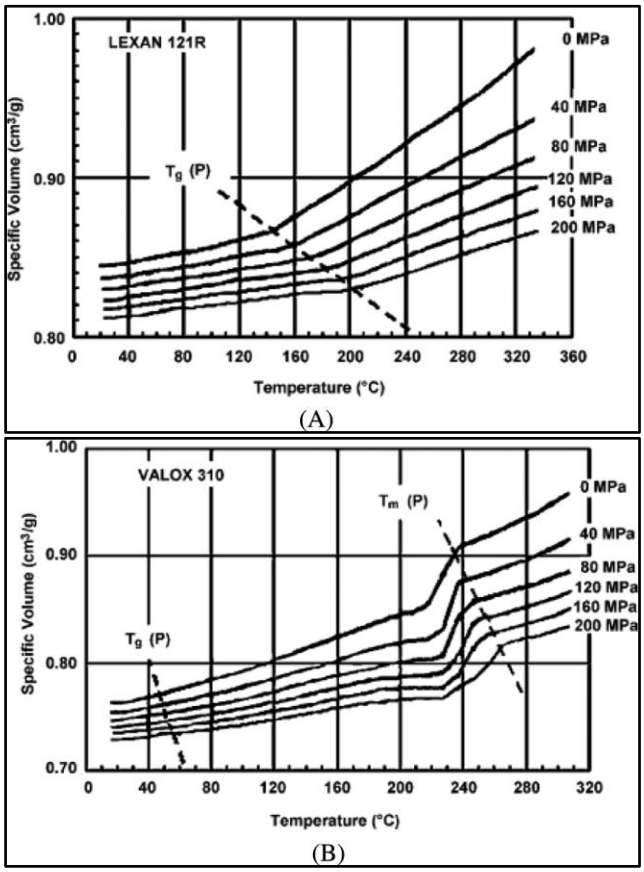

Figure 5: pvT-diagram of an amorphous (A) and a semi-crystalline (B) thermoplastic material [39].

The pvT measurement device consists of two pistons, a heated cylinder, and two polytetrafluoroethylene (PTFE) seals (see Figure 6). At first, the material is fed either in the form of pellets or powder into the heated cylinder. The PTFE seals ensure proper sealing of the material inside the heated cylinder. After setting the temperature, pressure and measuring intervals, the upper piston is lowered, the material is melted and the melt is compressed inside the cylinder at constant pressure. While the temperature is decreased at a constant rate of 6 K/min, the linear displacement transducer measures the contraction due to shrinkage of the material inside the chamber. The change in specific volume is calculated by measuring the change of the displacement of the piston and the mass of the specimen [72].

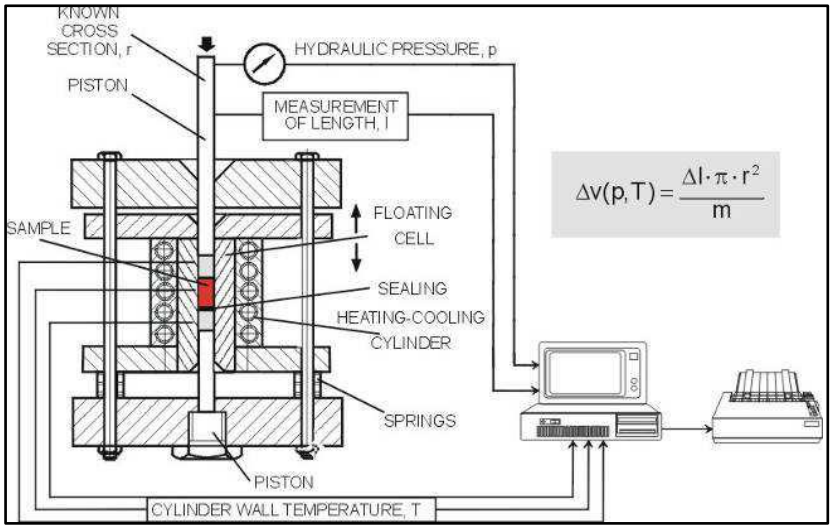

Figure 6: Schematic diagram of PVT100 (SWO Polymertechnik GmbH) [72].

2.3.2 Ways to reduce the shrinkage

Inorganic powders, flakes and fibres are generally incorporated into plastic resins in order to selectively modify the mechanical properties of the resin or to reduce the material costs. A secondary effect of using filler systems is that the composite of filler and resin will have a different shrinkage from the base polymer. Most fillers and reinforcements used in polymers are inorganic and have relatively low coefficients of thermal expansion (CTE), resulting in a decrease of shrinkages as well. The reduction in shrinkage is approximately proportional to the concentration of filler loading.

Overall, shrinkage can be controlled by means of incorporating fillers in the base polymer. A composite that exhibits lower internal stresses, uniformal shrinkage, and low warpage tendency can be produced by controlling the type, shape and level of reinforcement.

Fillers with low aspect ratio, defined as the ratio of the filler length to its diameter, can lead to isotropic shrinkage. Low aspect ratio fillers (e.g. spheres) ha the same dimension, so for this reason they tend not to get oriented along the flow direction, resulting in an improved dimensional stability. Low aspect ratio fillers do little other than occupy volume in the composite. As a result, they decrease the shrinkage in all directions equally [7, 15, 35, 36, 77].

Another method to improve the dimensional stability of a compound is to copolymerize or blend it with amorphous resins. Thereby the degree of crystallinity of the polymeric part of the compound will be reduced, which can result in a lower amount of change of specific volume during chain relaxation [2, 15, 28, 66].

2.4 Tensile Testing

Among all the properties of polymer, the mechanical properties are the most important properties, because practically all service conditions and the majority of the end-use applications involve some degree of mechanical loading. The material selection for a variety of applications is mostly based on mechanical properties, such as tensile strength, modulus, elongation, and impact strength.

Tensile elongation at break, strength and modulus are among the most important mechanical parameters of a material and are the most widely specified properties of plastic materials. All three parameters can be measured by means of tensile testing. Tensile strength or yield strength is a measurement of the ability of a material to withstand forces that tend to pull it apart and to determine to what extent the material stretches before breaking.

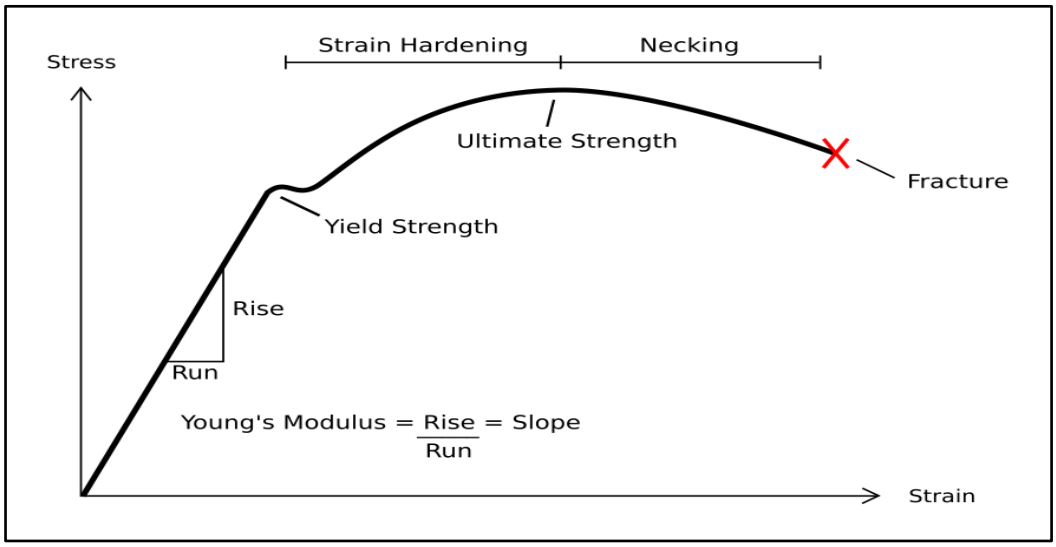

Figure 7: Stress-Strain curve and its calculations by graphical method [9, 63]

Often referred to as Young's modulus, or the modulus of elasticity, tensile modulus can be calculated using two methods, Tangent modulus and Secant modulus. Calculating Young's modulus via Tangent modulus is often done by taking slope (stress / strain) of the best possible straight line that can be fitted to initial portion of the curve starting from origin of the graph (see equation (3)). The secant modulus is usually calculated at a specified strain value, the slope of a secant line between 0,05 % and 1 % strain on a stress-strain plot and 1 % being commonly used for rigid materials [9] (see equation (4))

The nominal stress is

$$\sigma = \frac{F}{A_0} \qquad (1)$$

with F the tensile force and A_0 the initial area, while the nominal strain is defined as

$$\varepsilon = \frac{\Delta L}{L_0} \qquad (2)$$

The tangent modulus E_T is defined as

$$E_T = \frac{\sigma}{\varepsilon} \qquad (3)$$

and the often used secant modulus as:

$$E_{1\%}S = \frac{\sigma_2 - \sigma_1}{\varepsilon_2 - \varepsilon_1} \qquad (4)$$

whereby ε_1 lies between 0.0005 and 0.01 %.

The testing equipment consists of a fixed or essentially stationary clamping carrying one grip, and a movable clamping carrying a second one. Self-aligning grips/manually tightened for holding the test specimen between the fixed member and the movable teeth prevent alignment problems.

The speed of testing is the relative rate of motion of the grips or test fixtures during the test. The test specimen is positioned vertically in the grips of the testing machine. The grips are tightened evenly and firmly to prevent any slippage. The speed of testing is set at the proper rate and the machine is started. As the specimen elongates the resistance of the specimen increases and is detected by a load cell. This load value (force) is recorded by the instrument. The elongation of the specimen is continued until a rupture of the specimen is observed. Load value at break is also recorded. The tensile strength at yield and at break (ultimate tensile strength) are calculated [9, 20]

2.5 DSC

The term thermal characterization is frequently used to describe analytical experimental techniques which investigate the behaviour of a sample as a function of temperature. The thermal properties of polymer resins are equally as important as the mechanical properties. As polymer resins are extremely sensitive to temperature, properties such as mechanical,

chemical or electrical properties cannot be derived or investigated without characterizing the thermal property of the polymer resin. Crystallinity tends to induce important effects upon the thermal properties of a polymer, such as the sharp melting point and the stiffening of thermal mechanical properties.

In differential scanning calorimetry (DSC), the heat flow rate (differential power) is measured while the temperature of the sample changes, in a specified atmosphere. Because all materials have a finite heat capacity, heating or cooling a sample specimen results in a flow of heat, as endothermic and exothermic sample. Aforementioned we can investigate the change in heat capacity of the given polymer based on the release/consumption of energy. During the heating cycle the sample undergoes endothermic reaction, consuming the energy leading to investigate the melting point, T_M, and evaporation, similarly during cooling cycle the release of energy in terms of temperature i.e., exothermic reaction, provides the crystallinity point, degradation point and curing processes [9].

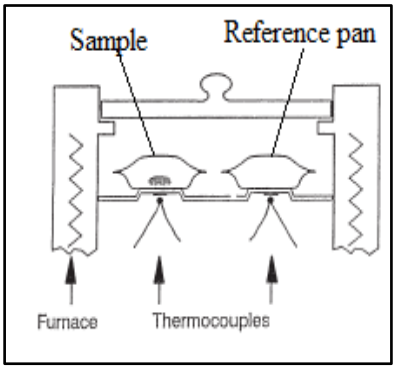

Figure 8: Typical representation of generic DSC chamber [63, 65]

A DSC contains two sample holders, each provided with its own heater as shown in Figure 8. The actual sample is placed in one of the sample holders in an aluminium pan and the other sample holder contains an empty pan (reference material, air). The temperature of both the sample holders is increased at a constant rate, such as 10 K/min, and we measure the difference in the energy H supplied to the two pans to keep them at the same temperature at all times. [27]. If the specimen and the reference material respond to the applied temperature profile in the same way, the heat flow remains constant. As aforementioned for the specimen during the endothermic processes, it requires additional heat to maintain the same temperature as the reference material. Hence, the heat flow increases, illustrated as an endothermic decrease in a DSC curve. During exothermic process, an increase in higher specimen

temperature is observed to that of the reference material. Thus, the heat flow decreases, which are reflected as exothermal increase in DSC curve [20, 23, 65] (see Figure 9).

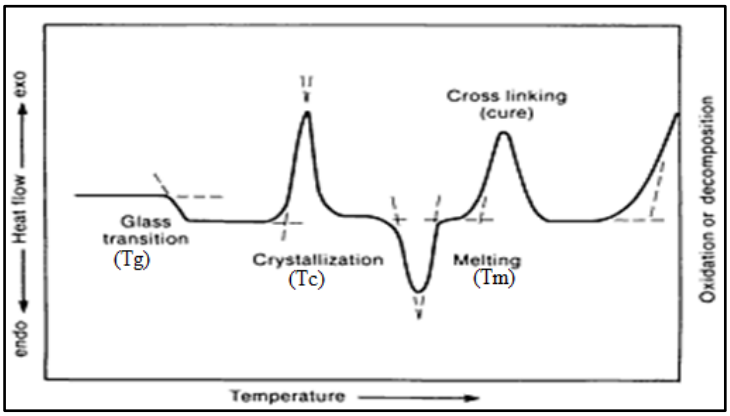

Figure 9: Typical DSC curve shown for four critical points, T_g, T_c, T_m, and cross linking [52]

2.6 Rheology

Rheology is defined as science of deformation and flow, where the term “rheos” meaning “flow” derived from Greek. Rheology is the study of flow behaviour of liquids and deformation behaviour of solids. Rheologically, all forms of shear behaviour is scientifically explained in between two regions i.e., the flow of ideal viscous liquids on one side and the deformation of ideal elastic solids on the other [43].

Rheometry is the measuring technology used to define measured rheological data. There are two types of equipment to investigate both liquids and solids using rotational and oscillatory rheometers.

Viscosity, during flowing of fluids, relative motion is observed between molecules resulting in generation of internal frictional forces. Therefore there is always a certain amount of resistance to flow which may be determined by viscosity.

Shear viscosity η (Pa·s) for ideal viscous fluids is defined as, when measured at constant temperature, the value of the ratio of the shear stress τ and shear rate $\dot{\gamma}$ is a material constant as shown in equation (5).

$$\eta = \frac{\tau}{\dot{\gamma}} \qquad (5)$$

In oscillatory rheometers, a two-plate model where the sample is sheared between the plates, the distance between two parallel plates is called shear gap. Whereas, the upper plate with the shear area A is set in motion by shear force F and the resulting velocity is measured while the lower plate being stationary (v = 0). In practice following shear condition assumptions are made for this test, and they are:

- The sample adheres to both plates and does not slide or slip.
- The sample is deformed homogeneously throughout the entire shear gap.

Viscoelastic materials, such as polymers, behave partly viscous and partly elastic whenever stress is applied. As a result viscosity of polymers is generally determined in terms of complex viscosity η* shown in equation (6)

$$\eta^* = \frac{1}{\omega} \cdot \left(G'' - i \cdot G'\right) \qquad (6)$$

Where ω is the angular frequency, the storage modulus G' is defined as a measure of the deformation energy stored by the sample during the shearing. G' represents the elastic behaviour of polymer.

Loss modulus G" is defined as the measure of the deformation energy used up by the sample during the shearing. When the polymer is flowing, frictional heat is generated due to relative motion between the molecules. A part of the energy is induced to the polymer for heating up and the part may be lost to environment in the form of heat. Energy lost in polymer shows irreversible deformation behaviour due to the changed shape after a number of strain cycle. Consequently, G" represents the viscous behaviour.

2.7 State of the art

2.7.1 Glass beads as a filler for polymers

Commercially available glass beads can be purchased in different sizes, configurations (hollow or solid) and with various coatings. Glass beads sometimes called microbeads, are incorporated into polymers to improve their stiffness [19, 68], surface resistance, dimensional stability [19, 49] and tensile strength [19, 47]. Moreover, glass beads influence the shrinkage behaviour of the compound drastically. They make the shrinkage of the compound more isotropic, which is not the case with sole fiber reinforcement [19, 47, 49].

Yuan et al. [80] reported that the size of micro beads strongly affects the compound's mechanical properties. The smaller sized beads increased the notched-Izod impact strength and the tensile strength considerably compared to larger sized beads. This may be due to the increased interfacial adhesion between particles and matrix [41, 78, 80].

Due to the inorganic nature of the uncoated glass beads, it is impossible to achieve adequate cohesion between the polymer and the filler. However, glass beads coated with silane coupling agents improve the hydrophilicity of the filler and therefore enhance the matrix-filler-cohesion. Hence, as investigated by Li et al. [31] silane coated glass beads improve the impact and tensile strength by about 40 % compared to untreated microsphere compounds [32, 34, 77]. Tolinski et al. [68]found out that coupling agents also increase the elongation at break dramatically and reduce the sphere breakage during processing [19, 31, 32, 34].

2.7.2 Glass beads in PP

Liang et al. [35] investigated the effect of glass beads with differnt diameters (4 µm, 35 µm, 219 µm) on the viscoelastic behaviour of PP. The authors had a closer look on the influence of fillers on the mechanical and thermal properties of the composite. The authors inferred that the experiment conducted at ambient temperature increased flexural storage modulus and loss modulus of the PP-glass beads non-linearly with increasing the volume fraction of glass beads. Additionally, the dynamic moduli of the compound increased with larger sized glass beads, when compared to smaller sized glass beads. The authors also reported that the glass transition temperature of the compound slightly increased linearly when the glass beads concentration was between 5 % and 15 %.

Liang [38] investigated the effect of large sized glass beads with a medium diameter of 219 µm on PP. The author conducted experiments to study the die swell behaviour and entrance pressure drop due to the fact that they influence elastic properties of polymeric melt during die extrusion. The author reported that the die swell decreased non-linearly with an increase in volume fraction of the glass beads.

Further studies are required to better understand the effect of glass beads on the mechanical behaviour and the crystallinity of the compound. Furthermore, there is the need to investigate the effect of compatibilizer on the interfacial adhesion between the filler and the polymer matrix. Finally, it is also necessary to investigate the above effects on the flowability, crystallinity and volumetric shrinkage.

2.7.3 Polypropylene in FFF

PP would be an ideal material for FFF, as it exhibits excellent mechanical properties, well-known processability and the base-polymer is much cheaper than currently available materials such as PLA, ABS or ABS/PC. However, PP has its inherent limitations such as high shrinkage due to semi-crystalline nature and high thermal expansion coefficient which limit its high temperature applications.

Apparently, only two research groups have been conducted research on polypropylene. Carneiro et al. [10] investigated the usage of neat PP and GF reinforced PP (GRPP) in FFF. The authors compared the mechanical properties of printed parts to parts that were compression molded. Additionally, the authors investigated the ideal process parameters for best printability of the parts on the heated bed. Carneiro et al. reported that the loss in mechanical performance of the printed sample was approximately 20-30 % in comparison to the compression molded sample. However, it was also reported that the sample printed at 0° orientation showed less than 20 % reduction in mechanical properties when compared to compression molding. Furthermore, it was found that there is an increase of around 30 % in modulus and 40 % in strength for the printed GRPP sample to that of neat PP. This means that the glass fibers maintained the reinforcing nature, even after extrusion. Although this publication only involved the printability of PP, they have not focused on how to optimize the material's intrinsic shrinkage, which could have optimized the warpage of the print even more. Moreover, they have not mentioned ways to deal with the anisotropic shrinkage in the GRPP.

Volpato et al. [71] investigated the effect of material degradation of PP in the printer head on the filament strength by means of tensile tests. The authors developed a piston-driven extrusion head to extrude filaments via pellets. Moreover, a method to reduce the effect of material degradation was under investigation.

Our research gives the unique opportunity to characterize and print PP reinforced with glass beads with different compositions, as the previous research only dealt with GF-reinforced PP and neat PP. Furthermore, both publications have not focused on the shrinkage and warpage issue. This research work will provide us a detailed insight into the shrinkage and warpage analysis of printed PP filled with glass beads and the issues arising during the different processing steps.

2.7.4 Compounds in FFF

The main objective of using compounds in FFF is to fabricate parts with high structural integrity, such as in dental replacements [11], replacements of artificial metal implants [60], and for drug delivery systems.

Highly filled metal composites filled for example with tungsten, ferromagnetic materials [61, 62], ceramics [26], iron powder, [42, 55] and copper [55], have been under investigation in the application for FFF. Moreover, fiber-reinforced polymers used in FFF for example filled with carbon fibers [56, 58, 67], glass fibers [81], or wood [17, 24, 25] have been studied so far.

Until now, only few researches has been published on compounds filled with lower aspect-ratio fillers (short fibers, beads, powders) with low filling rate. Dul et al. [12] published on thermo-mechanical behaviour of graphene nanoplatelets filled ABS. It is reported that the presence of graphene nanoplatelets influenced the improvement in tensile test and its positive effects on the different orientations of FDM samples (horizontal, vertical and perpendicular). However, the graphene nanoplatelets also exhibit loss in ultimate tensile strength and strain at break along the horizontal and vertical direction and a more severe loss in the perpendicular direction based on printing direction. The authors also infer that graphene nanoplatelets reduced the coefficient of thermal expansion of printed samples thereby improving their stability under long lasting loads.

Weng et al. [73] investigated the thermal and mechanical properties, as well as the morphology of ABS filled with organo-montmorillonite (OMMT) nano plates. Although the authors inferred the influence of nano-fillers to less or no warping and deformation in the printed product due to lower linear thermal expansion ratio of the composite, the true shrinkage data was not included.

The melt compounding of glass beads of different size and composition with PP will be interesting for checking the influence on shrinkage and printing property. The investigation of mechanical properties and filament extrusion of glass bead filled PP will be attractive for research work and may become a basis for the future research done in this particular area.

2.7.5 Blends used in FFF

In order to improve the application of FFF, it is essential to remove obsolete polymers with poor physical properties. One way to improve the properties of FFF products is to blend the polymer matrix with other polymers with superior or inferior properties to achieve appropriate properties based on the application. Roberson et al. [61] investigated different ratios of novel polycarbonate/styrene ethylene butylene styrene grafted with MA (SEBS-g-MA) compounds and studied the influence of different ratios of blending on the physical properties, extrusion parameters and melt flowability for the application in FFF.

Rocha et al. [62] conducted the study on binary and ternary polymeric blends of ABS, SEBS and ultra-high molecular weight polyethylene (UHMW-PE) to increase the variety of materials used in FFF. In order to improve impact toughness and abrasion resistance, the authors investigated the addition of UHMW-PE to ABS compatibilized by SEBS. Moreover, this publication described a method to improve the surface smoothness with different ratio of ABS-UHMW-PE-SEBS blends. Due to the fact that UHMW-PE is not extrudeable, the authors were not able to extrude filaments for weight concentrations of UHMW-PE greater than 25 %.

Ramli et al. [60] investigated the incorporation of UHMW-PE in HDPE with processing aids such as polyethylene glycol (PEG) to process in FFF in order to eliminate the metallic wear in artificial implants. Powdered UHMW-PE was blended with HDPE without a compatibilizer. The author achieved a reduction of the melt flow rate (MFR) by incorporating 60 % HDPE fraction in UHMWPE. Due to excellent processing property of the HDPE and also by incorporation of PEG as a processing aid it influenced the internal lubrication of UHMW-PE. Moreover, with a 50:50 ratio of UHMW-PE and HDPE the author was able to extrude filaments without any variation in filament dimension.

The state of the art research deals only with improvements in mechanical properties of blends without any indication of effects on the compound's crystallinity or shrinkage. Our research work will go one step forward, by blending flexible components with PP in order to facilitate the filament production of filled compounds. Moreover, the influence of blends on shrinkage, crystallinity and mechanical properties of the compounds will be studied. There are next to nil publications on TPE, amorphous polyolefin and amorphous polyamide based blending system for GB filled system.

3 Experimental

3.1 Materials

The base polymer with its trade name BD212CF was purchased from Borealis AG, Austria. Its physical properties are summarized in Table 1.

Table 1: Physical properties of PP-BD212CF [50].

Property	**Typical value**	**Test method**
Melt flow rate (230 °C/2.16 kg)	5 g/10 min	ISO 1133
Flexural modulus	950 MPa	ISO 178
Melting temperature-DSC	166 °C	ISO 11357-3

The glass beads Potter Spheriglass® were supplied by Potters Europe, Germany. Two different glass types were used: type E, which is an inorganic boro-silicate glass and type A, which is an inorganic soda lime glass. Their properties are summarized in Table 2. Both filler types were supplied in an unmodified form or coated with a silane coating optimized for PP.

Table 2: Properties of the Potters glass beads [51].

Property	**Type A**	**Type E**	**Test method**
Composition	Inorganic soda lime glass	Inorganic boro-silicate glass	-
Physical form	Spherical, non-porous	Spherical, non-porous	-
Surface treatment	CP03, silane coupling agent	CP03, silane coupling agent	
Specific gravity	2.50 g/cm^3	2.54 g/cm^3	ISO 787/10
Softening point	730 °C	846 °C	-
Young's modulus	68.9 GPa	72.4 GPa	-

The different filler size distributions of the uncoated fillers were obtained by dynamic light scattering with a Mastersizer 2000, which data supplied by Potters Europe, Germany (Figure 10). The mean filler size for each filler type, abbreviated by D_{50} is represented by the dashed line.

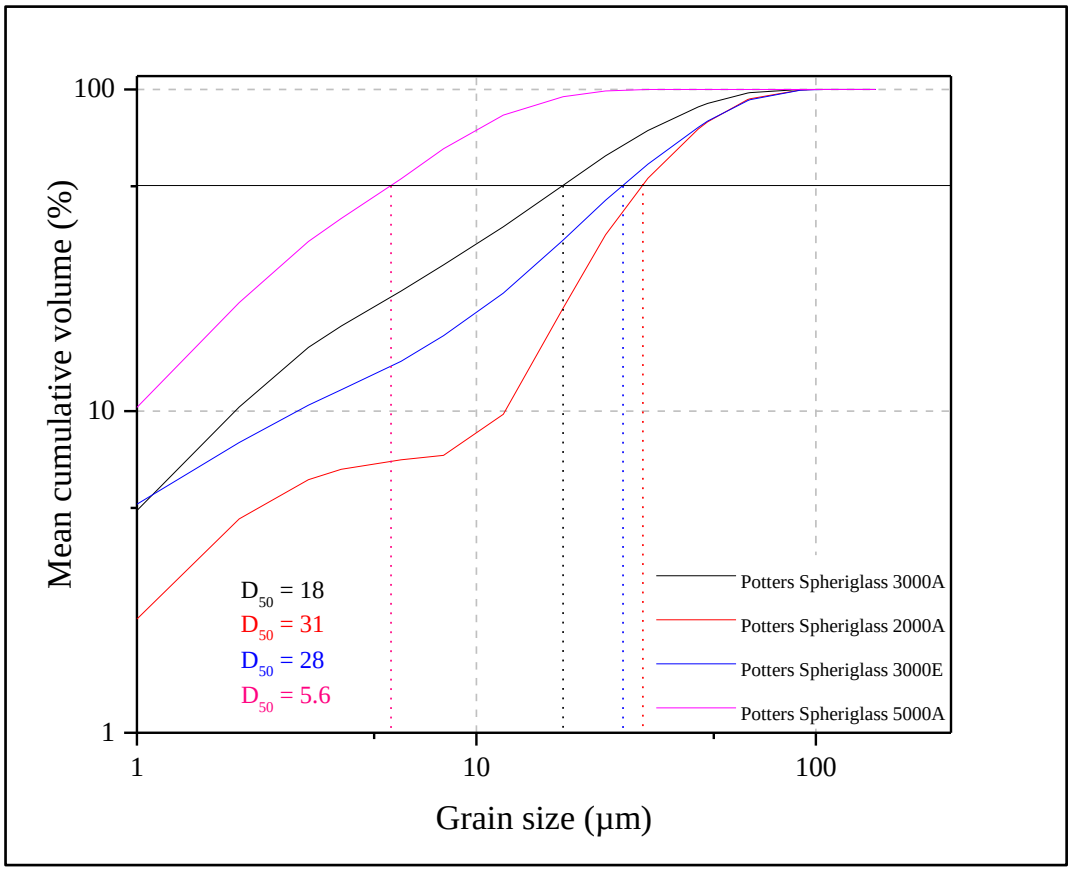

Figure 10: Particle size distribution and respective D_{50}-values of the fillers used.

In order to improve the compatibility of the polymer and the filler, the compatibilizer SCONA TPPP 9212 G (comp.) from BYK-Chemie GmbH, Germany, based on polypropylene functionalized with maleic acid anhydride, was used. It has a melt flow rate of 80 - 140 g/10min (190 °C, 2.16 kg) and a maleic anhydride content of ≥ 1.8 %.

In order to increase the elasticity of the filled compounds the following amorphous polymers were blended to PP:

- The amorphous polyamide (am.PA) Macromelt 6797 (Table 3) by Henkel AG & Co. KGaA, Germany,
- The styrenic thermoplastic elastomer (TPE) THERMOLAST® K TF6TAA, (Table 4) by Kraiburg TPE, Germany,

- The amorphous polyolefin (am.PO) Aerafin™ 180 (Table 5) by Eastman Chemical Company, USA, which is a fully saturated, low molecular weight, propylene-based olefin polymer [48].

Table 3: Properties of am.PA [53].

Properties	**Typical Value**	**Test Method**
Yield strength	1.2 N/mm^2	DIN 53455
Tensile strength	1.3 N/mm^2	DIN 53455
Break strength	0.7 N/mm^2	DIN 53455
Application temperature	180 – 220 °C	-

Table 4: Properties of TPE [54].

Properties	**Typical Value**	**Test Method**
Density	0.94 g/cm^3	DIN EN ISO 1183-1
Tensile strength	19.5 MPa	DIN 53504/ISO 37
Elongation at break	600 %	DIN 53504/ISO 37
Application temperature	180 – 220 °C	-

Table 5: Properties of am.PO [48].

Properties	**Typical Value**	**Test Method**
Viscosity, Brookfield @ 190°C	18000 cP	ASTMD D 3236
Glass Transition Temperature	-38 °C	ASTM D 3418

3.2 Methods

3.2.1 Equipment

All the equipment utilized during this research work is summarized in Table 6 to Table 9.

Table 6: List of Polymer processing equipment.

Device	Description
Lab kneader	Plasti-Corder PL2000, Brabender GmbH & Co. KG, Germany Polylab Rheomix 3000 coupled with a Haake Rheocord counter-rotating twin-screw kneader
Cutting mill	SM200, Retsch GmbH, Germany), equipped with a sieve with square perforations of 4x4 mm^2 in area
pvT measuring device	pvT 100, SWO Polymertechnik GmbH, Germany
High pressure capillary rheometer (HPCR)	Rheograph 2002, Göttfert Werkstoff-Prüfmaschinen GmbH, Germany
Vaccum press	P200V, Dr. Collin GmbH, Germany
Plate-plate rheometer	Physica MCR 501, Anton Paar GmbH, Austria
Single screw extruder	FT-E20T-MP-IS, Dr. Collin GmbH, Germany together with a melt pump, cooling bath and haul-off unit
Filament diameter measuring equipment	Sikora Laser 2010T and an Ecocontrol 600 processor, Sikora AG, Germany
FFF Printer	Hage 3DpA2, Hage Sondermaschinenbau GmbH & Co KG, Austria

Table 7**:** Device for thermal analysis.

Device	**Description**
Differential scanning calorimetry (DSC)	DSC 1, STAR ® system and Gas controller GC200, Mettler Toledo GmbH, Switzerland

Table 8 Device for mechanical characterization.

Device	**Description**
Universal testing machine (UTM)	Zwick Z001 Zwick GmbH&Co.KG, Germany

Table 9 Device for optical characterization.

Device	**Description**
Scanning electron microscope (SEM)	Vega 3, Tescan Brno, s.r.o., Czech Republic
Warpage analyser	ShapeDrive SD-3 sensor, ShapeDrive GmbH, , Germany

3.2.2 Preparation of compounds

The compounds were melted and mixed in the lab kneader (Table 6) at a constant temperature of 200 °C, at 60 1/min for 30 min. The mixing sequence started with the addition of PP at 0 min, in order to allow the polymer to melt inside the chamber for 2 min. After that the compatibilizer, with a relative filling degree of 10 % of the filler's content, was added to the molten PP, in order to form a homogenized melt during 4 min of overall mixing time. At the end of the 4 min, the filler was incorporated into the molten compound, and then it was mixed for 30 min to homogenize the filler in the melt. Similarly, the mixing of blends was carried out by adding the blend as the second ingredient. For reference purposes, unfilled PP was prepared under the same conditions. The compounded material was allowed to cool down to room temperature and afterwards was milled to pellets in the cutting mill (Table 6).

A total number of 29 formulations with varying filler loadings, different filler sizes and fillers in coated (silane coating optimized for PP) and uncoated form were conducted (see Table 10). Out of that, a total of 9 blended compounds were formulated after a careful selection based on the mechanical, shrinkage and thermal data (Table 10).

The naming of all formulation was done in a systematic manner. The letter 'A or E' represents the filler glass type (Table 2). The abbreviation 'C or UC' represents whether the filler is coated (C) or not (UC). The numbers '5.6, 18, 28 or 31' refer to the D_{50} of the filler. The numbers '15 or 30' represents the filler content in vol.-%. The additional letters 'TPE, am.PO or am.PA' refer to the blended polymer. Except unfilled PP, A-UC31-30-no-comp. and E-UC28-30-no-comp, all other compounds were coupled with compatibilizer.

Table 10: List of all formulations

Sample designation	PP (vol. %)	Comp. (vol. %)	Filler D_{50} (µm) coated	Filler D_{50} (µm) uncoated	Filler (vol. %)	Blend type	Blend (vol. %)
Unfilled PP	100	-	-	-	-	-	-
PP + comp.	97.09	2.91	-	-	-	-	-
A-C5.6-15	83.74	1.26	5.60	-	15.00	-	-
A-UC5.6-15	83.74	1.26	-	5.60	15.00	-	-
A-C5.6-30	67.96	2.04	5.60	-	30.00	-	-
A-UC5.6-30	67.96	2.04	-	5.60	30.00	-	-
A-C18-15	83.74	1.26	18.00	-	15.00	-	-
A-UC18-15	83.74	1.26	-	18.00	15.00	-	-
A-C18-30	67.96	2.04	18.00	-	30.00	-	-
A-UC18-30	67.96	2.04	-	18.00	30.00	-	-
A-C31-15	83.74	1.26	31.00	-	15.00	-	-
A-UC31-15	83.74	1.26	-	31.00	15.00	-	-
A-C31-30	67.96	2.04	31.00	-	30.00	-	-

A-UC31-30	67.96	2.04	-	31.00	30.00	-	-
A-UC31-30-no-comp.	70	-	-	31.00	30.00	-	-
E-C28-15	83.74	1.26	28.00	-	15.00	-	-
E-UC28-15	83.74	1.26	-	28.00	15.00	-	-
E-C28-30	67.96	2.04	28.00	-	30.00	-	-
E-UC28-30	67.96	2.04	-	28.00	30.00	-	-
E-UC28-30-no-comp.	70	-	-	28.00	30.00	-	-
A-C5.6-30-TPE	61.17	2.04	5.60	-	30.00	TPE	6.80
A-C5.6-30-am.PO	61.17	2.04	5.60	-	30.00	am.PO	6.80
A-C5.6-30-am.PA	61.17	2.04	5.60	-	30.00	am.PA	6.80
E-C28-30-TPE	61.17	2.04	28.00	-	30.00	TPE	6.80
E-C28-30-am.PO	61.17	2.04	28.00	-	30.00	am.PO	6.80
E-C28-30-am.PA	61.17	2.04	28.00	-	30.00	am.PA	6.80
A-C31-30-TPE	61.17	2.04	31.00	-	30.00	TPE	6.80
A-C31-30-am.PO	61.17	2.04	31.00	-	30.00	am.PO	6.80
A-C31-30-am.PA	61.17	2.04	31.00	-	30.00	am.PA	6.80

3.2.3 Shrinkage analysis

The compounded material was tested in a pvT measuring device (Table 6), in which the change in specific volume was measured at a constant pressure and decreasing temperatures. All formulations (Table 10) were characterized from 260 °C to 40 °C at constant pressure of 200 bar and cooling rate of 6 K/min. For all the results, the shrinkage was calculated at 230 °C to erase the variations occurring during the initial compression stage. All formulations were subjected to three repetitions.

3.2.4 DSC

The crystallinity plays a detrimental role in polymer dimension stability, as crystallization induces shrinkage in polymers when undergoing phase changes. As the crystalline phase tries to orient the polymer chains during the transition from the molten to the solidified phase, it induces higher shrinkage.

The degrees of crystallinity, as well as the crystallization temperature were investigated by means of differential scanning calorimetry (DSC) (Table 7), to study the influence of filler and compatibilizer. All the test samples were weighed approximately 10±1 mg. The non-isothermal study was conducted with three temperature sequences in the range of 40 °C to 200 °C. The 1st sequence consisted of a heating run followed by a cooling run. The completing sequence finished with a 2nd heating run. The heating rate was fixed to 10 K/min and the cooling rate to 20 K/min.

According to Vidović et al. [70], the degree of crystallinity of filled systems was calculated by the melting enthalpy of the 2nd heating run with respect to the filler's mass fraction and the heat of fusion of 100 % crystalline PP, which was set to 207 J/g [69]. The integration limits to obtain the melting enthalpy were always set to 100 and 165 °C.

3.2.5 Preparation of filaments

Based on the pvT and DSC results the selected formulations were extruded at the HPCR (Table 6), to study whether the chosen formulations can be extruded or not and also for further mechanical characterizations. A round die of 2 mm in diameter and a length of 30 mm was used for the extrusion of the filaments. The barrel and the die temperature of the rheometer were set to 200 °C and it was operated at a constant piston speed of 1.5 – 2.0 mm/min depending on the filament's diameter. After the die a haul off unit was provided

with a polytetraflouroethylene (PTFE) conveyor belt to extrude filaments at a constant diameter of 1.75 mm. The extruded filaments were cut to a length of 10 mm for further mechanical characterization.

3.2.6 Tensile test of filaments

The tensile tests of the filaments were conducted on the universal testing machine (UTM) (Table 8) with a load cell capacity of 1 kN and with added pneumatic grips. The tests were carried out at room temperature with relative humidity of 50 %. An initial load of 0.1 MPa and 50 mm gauge length were set. A minimum of seven filaments per formulation were characterized at a constant strain rate of 10 mm/min until their failure.

3.2.7 Rheology measurements

The samples for rheology tests, which were 25 mm in diameter and 2 mm in thickness, were compressed in the vacuum press (Table 6) at 200 °C with a steady increase of load (maximum of 160 bar) over a period of 50 min. The viscosity of the compression molded selected materials was investigated in the plate-plate rheometer (Table 6) under continuous flow of nitrogen and at test temperatures of 200 °C. At a gap of 1 mm, the deformation was set in a way to ensure to measure in the material's viscoelastic region for a frequency range from 500 to 0.1 1/s. At least two repetitions per material were conducted in order to get meaningful and repeatable results.

3.2.8 Morphology analysis

The morphology of the cross-sections of selected composites were examined by SEM (Table 9) at various magnifications. The samples were subjected to a cryo-fracture; the filaments were placed inside liquid nitrogen for 10 s before rupturing. The ruptured filaments were placed on a carbon tape over the sample holder, and later on coated with gold for 100 s. The samples were then analyzed with an electron beam of 5 kV.

3.2.9 Upscaling of filament production

After careful evaluation of mechanical, shrinkage, thermal and morphological behaviour, one suitable compound, as well as unfilled PP were extruded on a single screw extruder (Table 6). In order to reveal continuous flow and pressure, the single screw extruder was equipped with

a melt pump set to a speed of 16 1/min. The heating zones of the extruder barrel and that of the melt pump were set to 180 °C. A die with a diameter of 1.9 mm and a length of 25.05 mm was used. To attain efficient cooling, after the die a water bath of 3 m in length and equipped with 40 °C warm water was placed. After the haul off unit, the filament diameter measuring equipment (Table 6) was used to measure and control the variation of diameter in the filament. When the diameter was set to 1.75±0.05 mm, constantly over time, the filament was winded on spools for subsequent printing.

3.2.10 Printing trials

The printing trials were carried out with the FFF printer (Table 6), with a brass nozzle of 0.5 mm in diameter. As PP is difficult to print on the typical printing bed surfaces (e.g. mirror or Polyimide tape), a pressed (Table 6) PP-plate (same grade as described above) was used as a printing bed surface. The printing bed temperature was set to 70 °C, and the die temperature to 210 °C. The printing layer height was set to 0.2 mm and a constant infill density was guaranteed. The printed part, used for the warpage analysis, was designed in a way (Figure 11) so that it is very prone to warpage. The model was sliced in the software Slic3r 1.2.8 created by Alessandro Ranellucci.

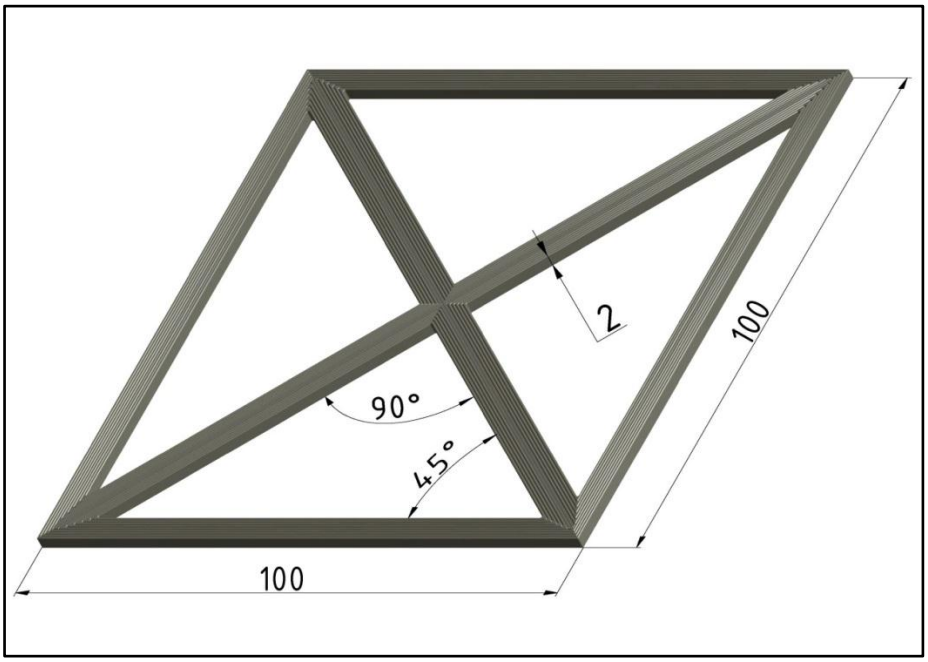

Figure 11: 3D CAD design for the warpage analysis shown with its dimensions in mm.

3.2.11 Warpage analysis

The printed parts were stored at room temperature and relative humidity of 50 % for two weeks to control the post crystallization. The warpage measurements of the printed samples were carried out by means of a ShapeDrive SD-3 sensor (Table 9), which is a 3D shape measuring tool, using a point cloud method to record a large number of points of the object's surface. The printed samples were measured at a working distance of 300 mm with a measurement interval of 2 s. The open source software CloudCompare version 2.6.1, developed by Daniel Girardeau-Montaut, was used, which is a 3D point cloud analyser, to compare the cloud data from the scan with that of the CAD file.

4 Results and Discussion

4.1 Compatibilized PP filled with glass beads

In this section, the detailed analysis of the research work was performed for varying filler content, filler type and with or without compatibilizer (Table 10). The influences on the shrinkage, thermal properties, mechanical properties, flow properties and their morphology are presented.

4.1.1 pvT analysis

The shrinkage behaviour of unfilled PP and the influence of filler content on compatibilized PP were investigated by means of pvT, in which the change in specific volume is equivalent to the materials shrinkage.

In Figure 12 the change in specific volume of unfilled PP (black curve) to that of A-C5.6-15 (PP + comp. + 15 vol. -% coated A-glass with a D_{50} of 5.6 µm) (red curve) and A-C5.6-30 (PP + comp. + 30 vol. -% coated A-glass with a D_{50} of 5.6 µm) (blue curve) (Table 10) is illustrated as a function of temperature. The y-axis is represented as the relative specific volume normalized to the specific volume at 40 °C, because with this representation the shrinkage progress over the temperature is clearly visible.

Figure 12 shows a decrease in specific volume with increasing filler content. The incorporation of filler results in a restriction of the movement of the polymer chains. Hence results in a reduced change in specific volume [30]. Furthermore, Figure 12 suggests that the GB content considerably restricts the strong specific volume change in a very short temperature range. This can be attributed to the crystallization region of PP. Due to the prevention of polymer chain orientations by the incorporated filler, the drastic change in specific volume is decreased. The shift of the crystalline transition to higher temperatures for the filled compounds (Figure 12) can be related to a nucleating effect of PP.

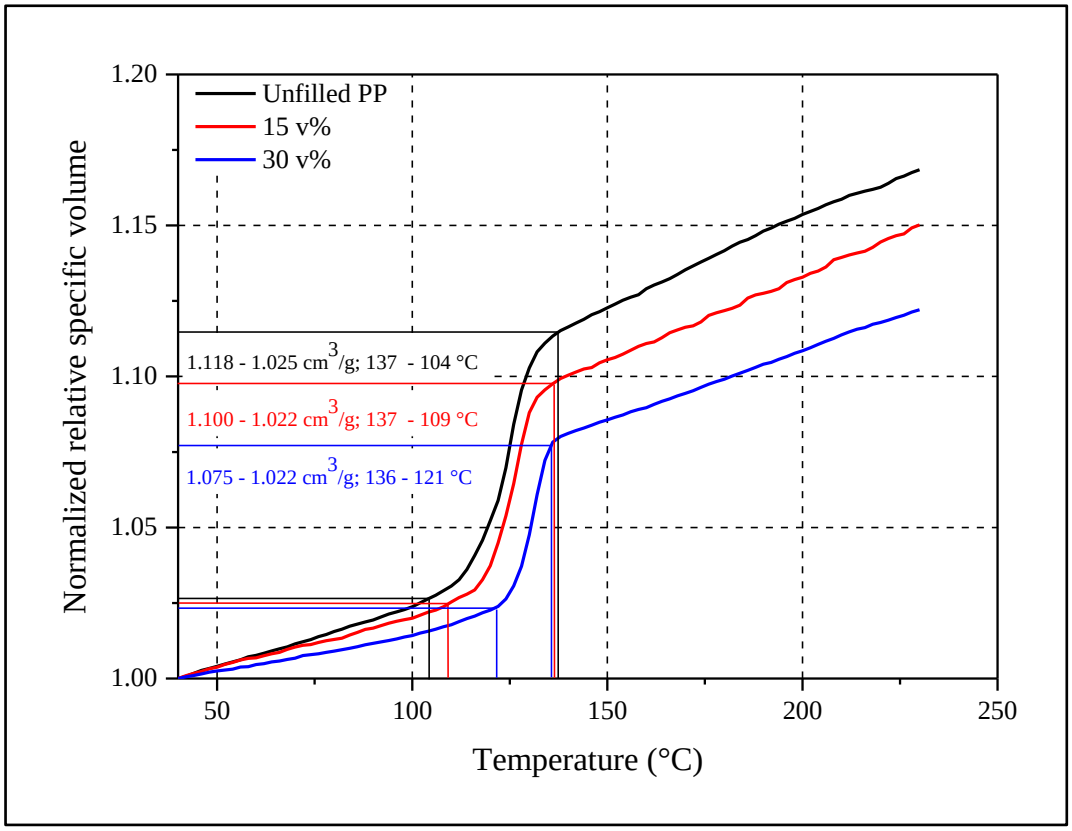

Figure 12: Normalized specific volume as a function of temperature and filler volume content of unfilled PP and PP+comp. filled with 15 vol.-% and 30 vol.-% of coated A-glass with a D_{50} of 5.6 µm at a constant pressure of 200 bar.

Figure 13 illustrates the shrinkage at 230 °C as a function of D_{50} for a filling degree of 15 vol.-% (a) and 30 vol.-% (b) for all filler types (Table 10). As expected and described above, the addition of 15 vol.-% of filler (Figure 13a) leads to a much smaller shrinkage reduction (around 11 % compared to PP) than the compounds consisting of 30 vol.-% (Figure 13b) (around 27 % compared to PP).

All data plots for the 15 vol.-% and 30 vol.-% compounds, respectively lie in the same region (14.85±0.2 % for 15 vol.-% filler content and 12.05±0.2 % for 30 vol.-% filler content) independent of the filler size. The deviations could be due to errors from the equipment. Hence, there is no relevant difference between the different D_{50}-values for a given filler content.

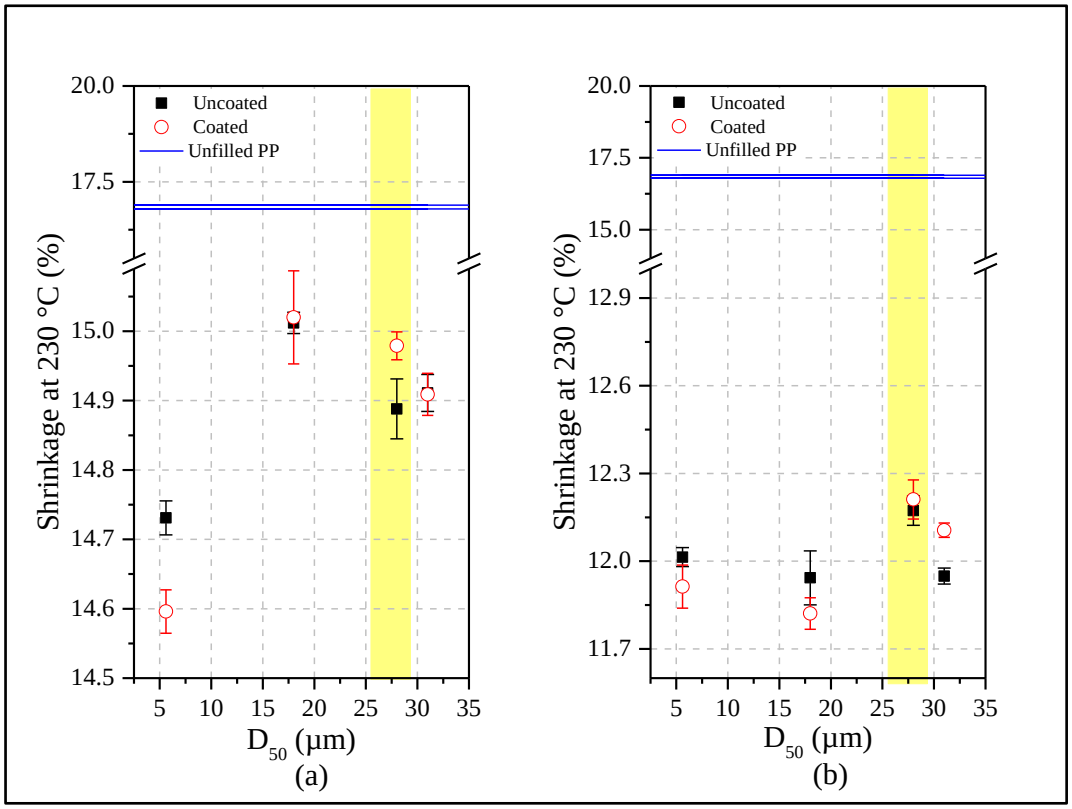

Figure 13: Mean and standard deviation of the shrinkage at 230 °C as a function of D_{50} for a filling degree of a15 vol.- % (a) and 30 vol.- % (b). The highlighted part refers to the filler type E, and the non-highlighted part to the A-glass-type. The blue lines represent the standard deviation of the shrinkage at 230 °C for unfilled PP.

By the above shrinkage results it is evident not to pursue formulation with 15 vol.- % of GB content which has not a relevant influence on shrinkage reduction when compared to 30 vol.- %. For 30 vol.- % both type of GB, shows promising result for reduction of maximum shrinkage % (12.0±0.2 %) in comparison with unfilled PP (17 %).

4.1.2 DSC analysis

In this chapter, the thermal behaviour of the samples were investigated by means of DSC in order to understand the influence of fillers. Figure 14 shows more or less a similar degree of crystallinity for both filled and unfilled systems. As a result, the possibility of interpreting the individual data trends for filled and unfilled system can be ruled out. Moreover, the differences between the compounds are well within the measurement tolerances of the measuring device (±3 %). In addition, this variation may also be related to sample preparation

[29], suggesting no significant change in crystallinity, which asserts the reduction in shrinkage.

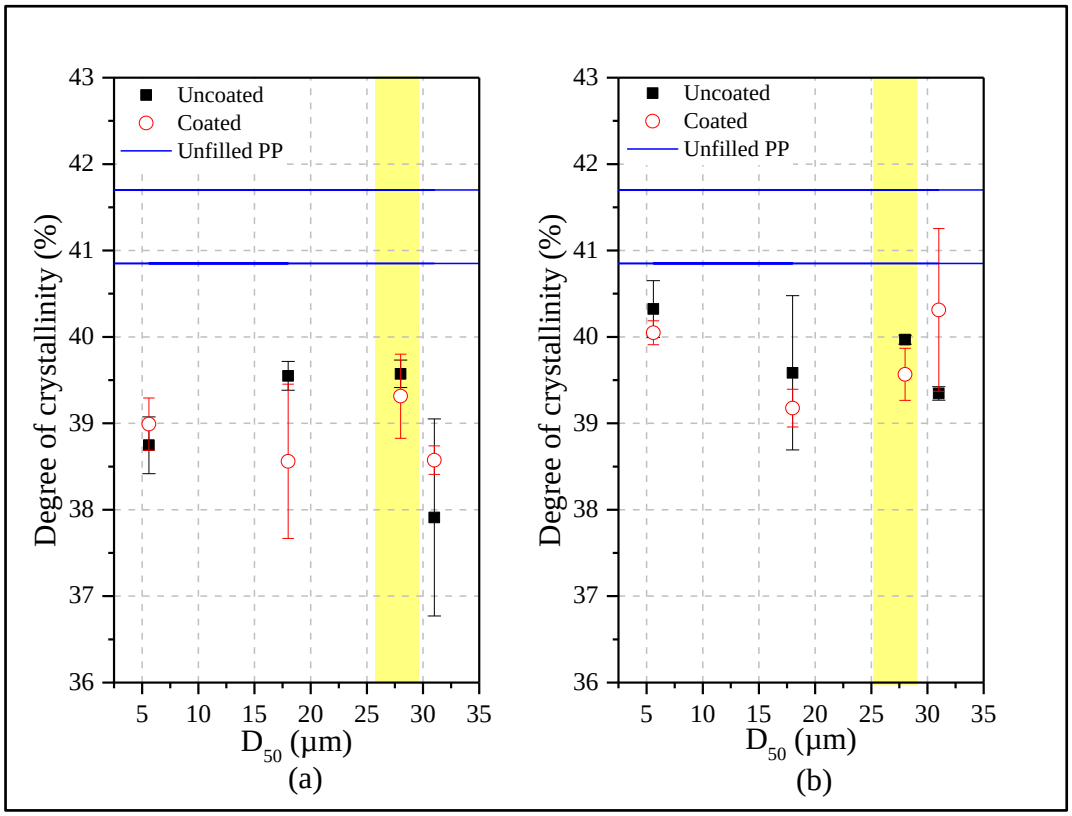

Figure 14: Mean and standard deviation of the degree of crystallinity as a function of D_{50} for a filling degree of 15 vol.-% (a) and 30 vol.-% (b). The highlighted part refers to the filler type E, and the non-highlighted part to the A glass-type. The blue lines represent the standard deviation of the degree of crystallinity for unfilled PP.

However, in the case of the crystallization temperature, Figure 15 shows not only for the compounds consisting of 30 vol.-% filler a drastic change in the crystallization temperature, but also at 15 vol.-% a slight increase. The reason for an increase in crystallization temperature with higher filler content could be the increase in nucleating sites. Yuan et al. [79] observed the similar trend for a GB size of 4 µm. The authors suggest that at 30 wt.-% or above, the GB content increases formation of nucleation sites [79].

The smaller sized fillers 5.6 µm exhibit a significantly higher nucleating activity especially for 30 vol.-% filler content (see Figure 15a and Figure 15b). This has also been observed in other studies [40, 44, 79], due to a larger total surface area, which increased the ability to form a bigger number of nucleation sites. Moreover, both uncoated E-glass types exhibit a considerable increase in crystallization temperature compared to the similar sized A-glass

compound, which could be related to the different chemical structure of the E-glass. Furthermore, the E-glass used has a higher content of smaller sized fractions (Figure 10), which can better act as nucleating agents than bigger sized particles.

According to Yuan et al. [79], the authors observed more pronounced β-nucleation sites in terms of crystallization temperature for a filler size of 4.0 µm and 35.0 µm both coated with silane coupling agent and suggests that the crystallization temperature for both filler types increased β -crystallization sites. In this research similar β -crystallization sites were found for both coated and uncoated A-type 5.6 µm, appears in 2nd heating cycle at around 148 °C to 154 °C and for both coated and uncoated E-type 28 µm, around 151 °C to 156 °C.

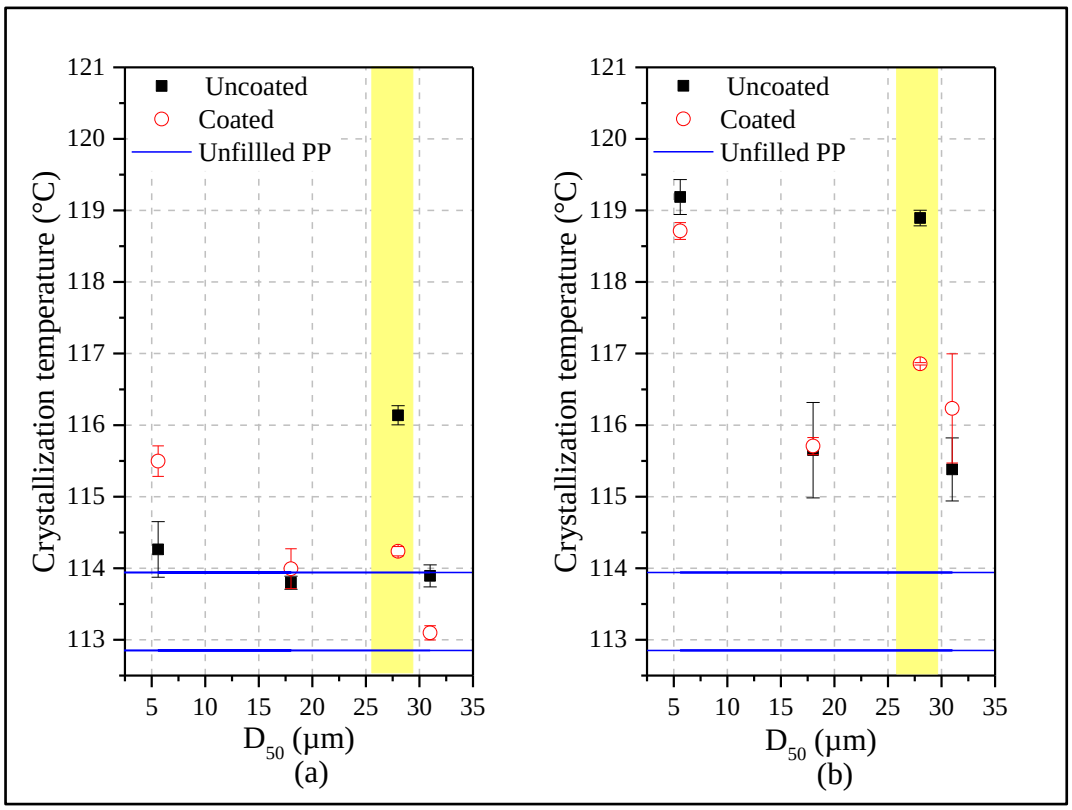

Figure 15: Mean and standard deviation of the crystallization temperature as function of D_{50} (µm), for filling degree 15 vol. -% (a) and 30 vol. -% (b). The highlighted part refers to the filler type E, and the non-highlighted part to A-glass type. The blue lines represent the standard deviation of crystallization temperature for unfilled PP.

The results obtained show relatively small change in crystallinity regardless of filler type and volume content, which indeed supports the good shrinkage reduction. The only appreciable change was observed in the case of the crystallisation temperatures that increase by 7 K in the small size of type A filler and the uncoated type E filler. In addition, an increased

crystallization temperature may assist in reducing and controlling the warpage of the printed part, as the polymer crystallizes much faster upon cooling. Thus, with increase in temperature, the polymer crystallizes earlier, thereby minimizing the cause and effect and resulting in a controlled change in specific volume.

4.1.3 Rheology

According to Spörk et al. [64], the viscosity of the material is not the prime parameter for printing, but still an important one. In order to achieve good printability, the authors infer that the material's viscosity should be approximately 1000 Pa·s or below for shear rates above 100 rad/s. Overall, the material should also possess certain amount of melt strength so as to avoid buckling and cause distortion during the deposition of the filament [64].

Figure 16 illustrates the viscosity as a function of angular frequency for the investigated materials. In Figure 16a, the curve for PP and PP+comp. shows a distinctive Newtonian plateau at low angular frequency, followed by a shear thinning non-Newtonian flow behaviour at elevated angular frequencies, typically for thermoplastic polymers [7, 14]. However, an overall decrease in viscosity for PP+compatiblizer is observed due to melt mixing of PP with a low viscous component (compatibilizer). This same behaviour has been reported by Balkan et al. [7] and Liang et al.[7, 37]. The uncoated filler tends to form agglomerates or network-like structures [7], as it does not have a good interaction with the polymer. This can be seen by means of the strong increase in viscosity for low angular frequencies for A-glass type 5.6 μm uncoated and by the overall elevated viscosity compared to the coated compound 5.6 μm coated. This suggests that the coating is effectively improving the dispersion of the filler and the interface between the polymer and the filler. So only at low angular frequencies 5.6 μm coated still tends to form agglomerates. At higher shear rates, its viscosity is significantly reduced (by 63 Pa·s) to that of the uncoated compound, but also lower than unfilled PP (by 10 Pa·s). This rather unexpected phenomenon might be explained by the so-called ball bearing effect, which has been found for compounds consisting of spherical fillers [7, 33, 75]. The interpartical gaps between adjacent rotating spheres can result in an elevated local shear. This may initiate interfacial slip and disentanglements of macromolecules, which results in a decline in viscosity [7, 33, 75]. The uncoated compound does not show the described decreased viscosity at higher shear rates, as the non-uniform distribution of the fillers does not promote the rotation of the spheres.

All compounds consisting of the bigger sized fillers (D_{50} ca. 30 µm) (Figure 16b) reveal an even more reduced viscosity for all shear rates compared to PP+comp. and to the compounds with smaller fillers (Figure 16a). This suggests that for bigger fillers the ball-bearing effect seems to be more prominent than for small fillers (Figure 16a). Moreover, all shown compounds appear to have a good distribution of the filler, since there is no big difference between the viscosities of the coated and uncoated grades. The slight increase in viscosity at lower shear rates can again be attributed to the formation of agglomerates [35].

To sum up, the investigated rheology results for D_{50} 5.6 µm, 31.0 µm and 28 µm are well within the minimal requirement for filament printing [64], which suggests that all compounds tend to be printable.

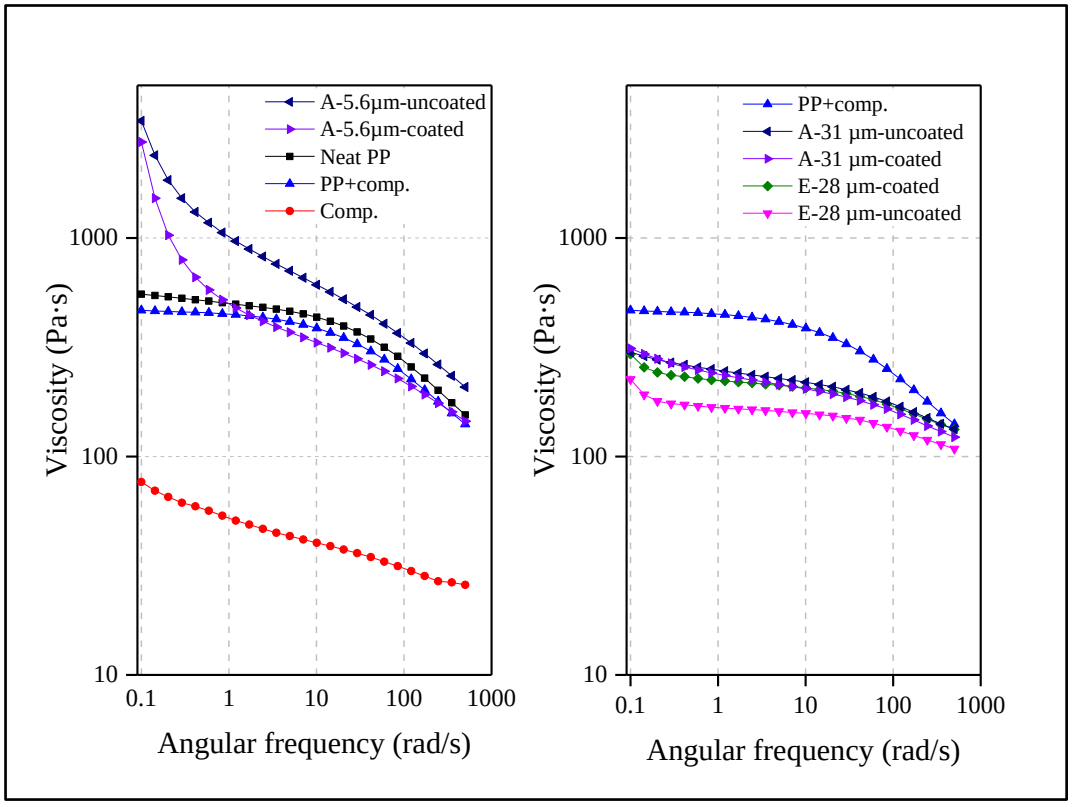

Figure 16: Viscosity as a function of angular frequency for the raw components and the compounds with a filler content of 30 vol. -% with a D50 of 5.6 µm (a), and for A- and E-glass type compounds of similar D50 (ca 30 µm) (b).

4.1.4 Tensile testing

The basic requisite for any filaments to print is to have high stiffness and yield stress, so as to avoid the buckling of the filament during printing. Additionally, the material should possess a

certain amount of flexibility for winding and storing the filament in spools. According to Spörk et al., [64] yield stress and the elongation at yield can strongly influence the mechanical response in the FFF process.

In Figure 17 the elongation at yield (a) and the yield stress (b) as a function of D_{50} is plotted. In order to understand the influence of the compatibilizer on the mechanical properties of selected components, compounds without compatibilizer are added, as well. Compared to neat PP, all compounds reveal a drastically reduced elongation at yield, as the increase in filler reduces the mobility of the chains, which negatively affects the orientation of the chains [59]. As result it restricts the chain slippage, resulting in poor ductility thereby reducing the elongation at yield. In addition Bai et al. [6] also observed that the elongation at yield is inversely proportional to the concentration of the rigid GB. Moreover, it can be seen that the elongation at yield improves with decreasing filler size, since smaller particles can take up higher stress concentrations at their interphase [32, 34]. For all filler sizes, the coated filler compounds reveal an increased elongation at yield compared to the uncoated ones, because of the chemical bonding between filler-coating and polymer [32]. In Figure 17a it is also evident that the E-glass type shows a much better compatibility to the polymer than the A-glass types. Even without compatibilizer the elongation at yield (1.55±0.16 %) is higher than the compatibilized compounds consisting of A-glass 31 µm uncoated (0.95±0.14 %) and coated (0.88±0.11 %). A drastic increase in the elasticity is observed, when the coated E-glass is combined with the compatibilizer.

In Figure 17b similar trends can be observed for the yield stress. The yield stress is increasing with smaller filler size, since smaller particles can take up higher stress concentrations at their interphase [16]. Again all coated filler compounds reveal the best yield stress due to the chemical bonding between the filler and the polymer. Compared to the A-glass type with biggest filler size, the compound with coated E-glass showed much higher filament yield stress values (20.56±0.57 MPa), which confirms the previously described improved compatibility between E-glass and PP. Especially the coating for the E-glass compound enhances the yield stress to a level close to unfilled PP. This implies that the coated filler seems to be well dispersed, and has better interaction between filler and matrix. Hence, it shows that the compatibilizer seems to interact in a more efficient way with the borosilicate glass surface coated with silane coupling agent than with the inorganic soda lime glass surface coated with the silane coupling agent.

According to Spörk et al. [64], unfilled PP is still extrudable in FFF and suggests that filaments with lower yield stress may be usable, if provided with sufficient elongation at yield. In line with the above reference the E-C28-30 (PP + comp. + 30 vol. -% coated E-glass with a D_{50} of 28 µm) A-C31-30 (PP + comp. + 30 vol. -% coated A-glass with a D_{50} of 31 µm) and A-C5.6-30 (PP + comp. + 30 vol. -% coated A-glass with a D_{50} of 5.6 µm) were chosen for further study with different blend composition in order to improve the processing conditions for filament extrusion and printing and also to improve filament elongation at yield.

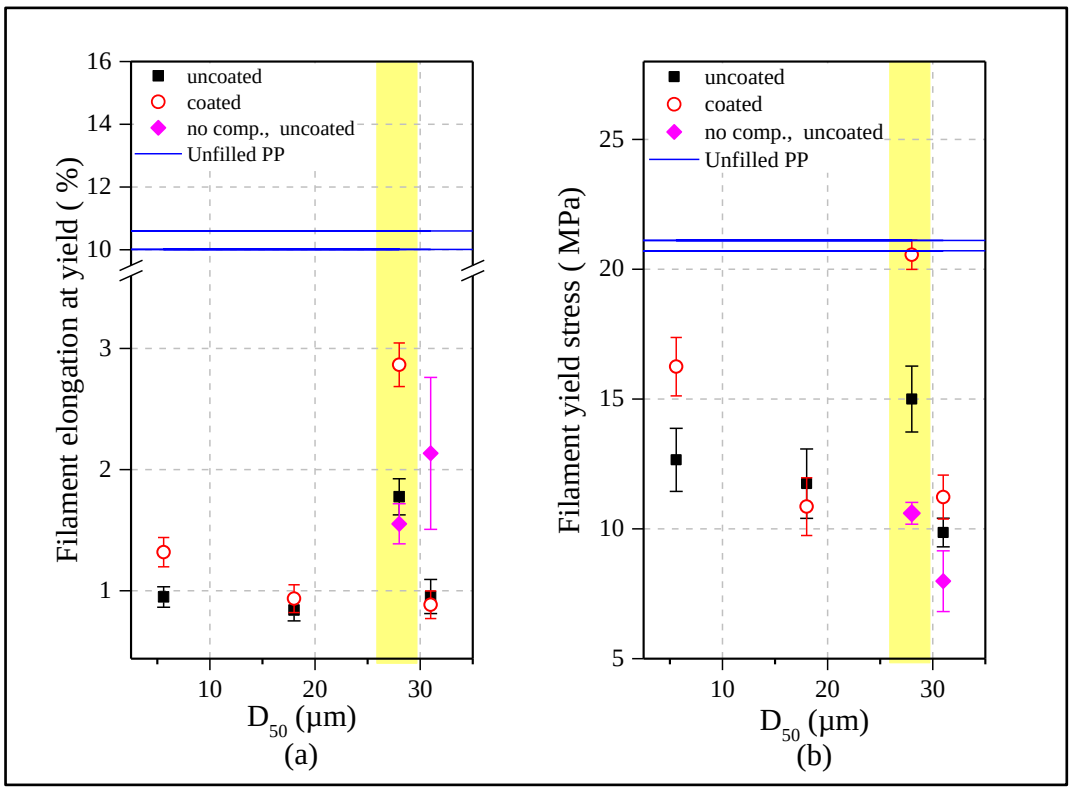

Figure 17: Mean and standard deviation of the filament elongation at yield (a) and the filament tensile strength (b) as a function of D_{50} for a filling degree of 30 vol.-%. The highlighted part refers to the filler type E, and the non-highlighted part to the A glass-type. The blue lines represent the standard deviation of the values for unfilled PP. For selected compounds, composites without compatibilizers were investigated, as well.

4.1.5 Morphology

Scanning electron microscopy (SEM) was used in order to investigate and study the interfacial adhesion between the inclusions and the matrix, as well as the particle distribution in the matrix. The SEM micrographs compare both the A-glass types and E-glass types in Figure 18 and Figure 19, respectively.

Figure 18 shows the cryo-fractured filaments of compounds consisting of A-glass types for both 31.0 μm (a) and 5.6 μm (b), coated with the silane coupling agent. The comparison of both micrographs indicates that the latter shows a much better dispersion and a more even distribution of filler in the polymer matrix due to smaller sized GB.

Figure 18a shows large and micro voids indicating poor adhesion between the filler and matrix. This behaviour is clearly explained by Li et al. [31] and Lian et al. [34]. Both authors suggest that it is fairly difficult to distribute larger sized GB uniformly in the matrix due to the fact that they are larger and along with the smooth surface they tend to slip. The authors also correlate this behaviour to the larger deviation in mechanical properties. Though the GB in PP is compatibilized, it shows very poor interaction between the filler and the matrix (large voids in Figure 18a), implying that the compatibilizer is not coupling well to the A-glass type, as mentioned in the previous section. However, when having a closer look to the bottom micrograph, it shows a contradicting perspective. The matrix shows some adhesion to GB and overlaps on the surface (Figure 18a). This phenomenon can be explained based on the broad size distribution of A-C-31-30 (PP + comp. + 30 vol. -% coated A-glass with a D_{50} of 30 μm). As the size distribution is broad, it indicates smaller sized GB may have influenced the interfacial adhesion. Moreover, this also implies that the 5.6 μm sized filler, which has a narrower size distribution than the filler with 31.0 μm (see Figure 10), this signifies that there is no presence of larger sized GB, causing no large voids during rupture (see Figure 18b). This result can also be related to the tensile properties, in which the compounds consisting of 5.6 μm show better results than the one with 31.0 μm.

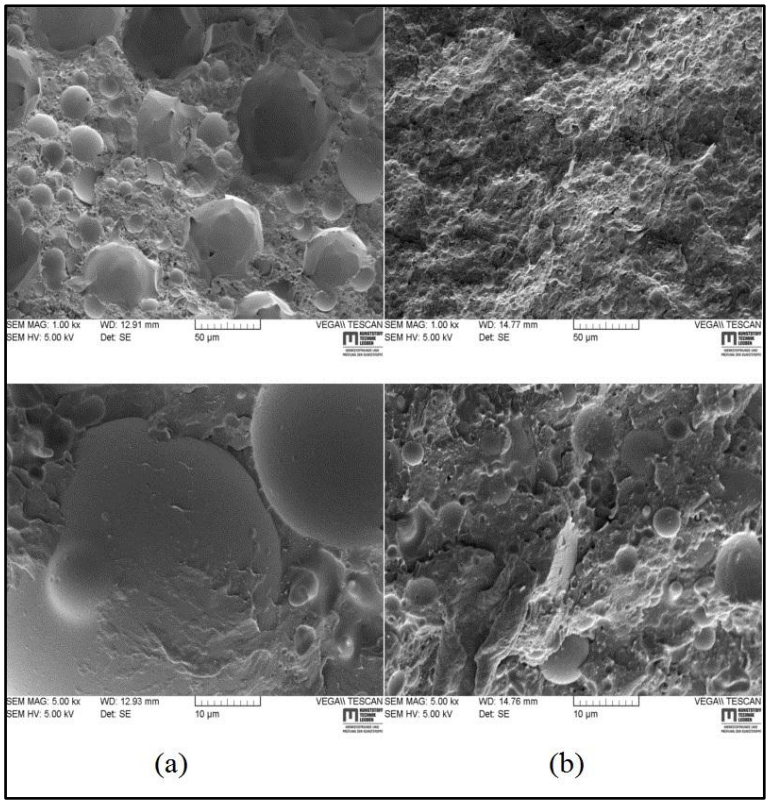

Figure 18: SEM micrographs of the A-C31-30 (PP + comp. + 30 vol. -% coated A-glass with a D_{50} of 31 μm) (a) -A-C5.6-30 (PP + comp. + 30 vol. -% coated A-glass with a D_{50} of 5.6 μm) (b) with the magnifications of 1000x (top) and 5000x (bottom).

In Figure 19a the compound E-C28-30 (PP + comp. + 30 vol. -% coated E-glass with a D_{50} of 28 μm) reveals an even distribution of fillers in the matrix. The interfacial adhesion seems to be superior when compared to the A-glass filler. The GB is found to be intact within the polymer matrix, as it overlaps with the polymer, indicating superior compatibilization with the matrix due to the coating and compatibilizer.

The micrographs of E-UC28-30 (PP + comp. + 30 vol. -% uncoated E-glass with a D_{50} of 28 μm) (Figure 19b) show a smoother surface than Figure 19a and an even distribution of fillers in the matrix. Similar to E-C28-30 (PP + comp. + 30 vol. -% coated E-glass with a D_{50} of 28 μm) (Figure 19a), the GBs remain intact within a polymer matrix even after rupture, indicating good compatibilization between the filler and the polymer. In the bottom micrograph the compound shows pronounced interaction between the filler and the matrix. The polymer matrix is overlapping the GB, resulting in an increase in tensile properties. Moreover, the increase in homogeneity in the filler distribution could have increased the nucleation sites and therefore the crystallization temperature (Figure 15b).

The uncompatibilized compound (Figure 19c) shows a homogenized filler distribution in the matrix. However, voids around the GB are clearly visible. This is most certainly related to the poor interaction between the matrix and the filler. Additionally, in the bottom micrograph, a magnified image provides a clear picture of filler-matrix interaction and very distinctive voids around the filler. This phenomenon contributes hugely to the big variances in tensile properties (Figure 17) between the compatibilized (20.55±0.57 MPa) and uncompatibilized grades (10.59±0.42 MPa) [6, 32, 34].

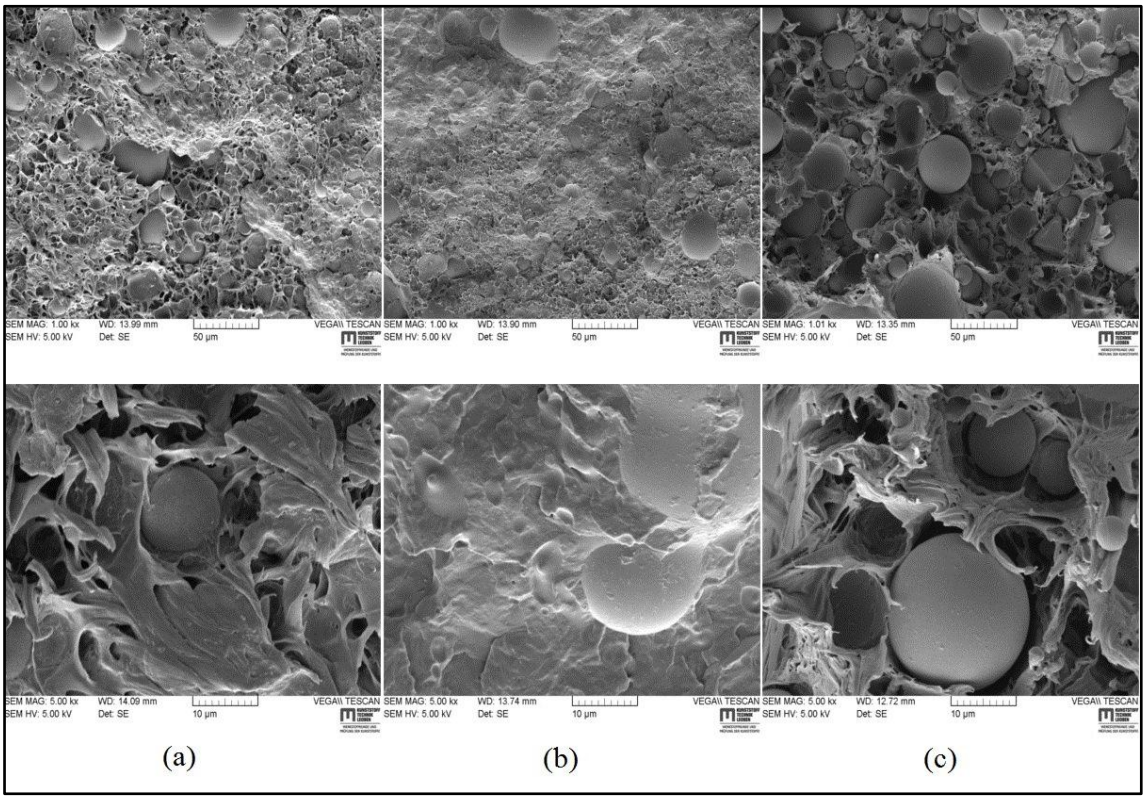

Figure 19: SEM micrographs of the compounds with E-C28-30 (PP + comp. + 30 vol. -% coated E-glass with a D_{50} of 28 µm) (a), E-UC28-30 (PP + comp. + 30 vol. -% uncoated E-glass with a D_{50} of 28 µm) (b) and E-UC28-30 without comp. (PP + 30 vol. -% uncoated E-glass with a D_{50} of 28 µm) (c), with the magnifications of 1000x (top) and 5000x (bottom).

The optical analysis carried out using the SEM revealed the differences in the morphology of the different compatibilized compounds and helped to describe the influences of tensile, flow and thermal properties. The optical analysis also helped in deciding the compounds for further investigation using blend materials.

4.2 Glass bead filled compatibilized PP with blends

In this section different blend materials and its influence on different properties are investigated. In the following subsection the results of pvT measurements for maximum shrinkage reduction, DSC measurements to study the influence of induced rubber phase into semi-crystalline phase and the influence on rheology and mechanical properties in co-relation with morphology are discussed.

4.2.1 pvT analysis

In Figure 20 the maximum shrinkage at 230 °C is plotted as a function of D_{50} for all blended compounds. The influence of rubber like material on PP + compatibilizer filled with GB was analyzed.

No relevant reduction in shrinkage for all blend types in comparison to that of filled PP without blends is observed. Moreover, no change in maximum shrinkage % between the different blend types is also visible, all blend type 11.5 ± 0.3 %. In addition, the below figure confirms that the addition of blends do not results negatively on the maximum shrinkage. In other words it shows no influence on the shrinkage reduction.

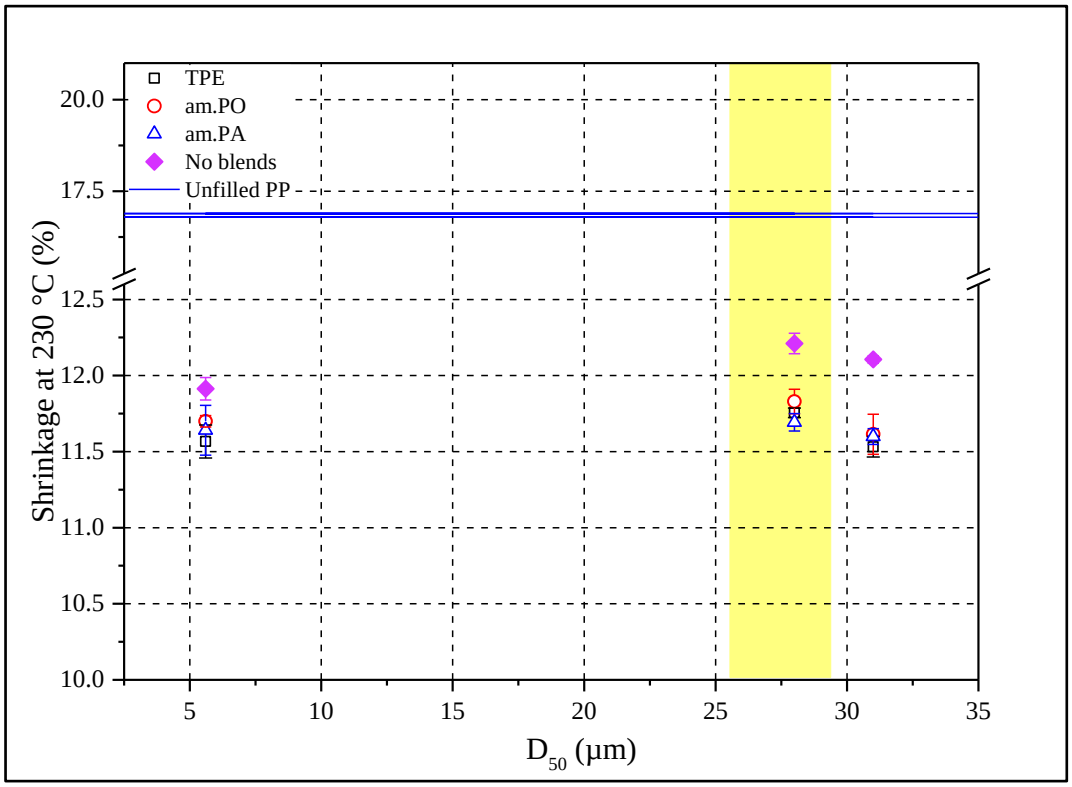

Figure 20: Mean and standard deviation of the shrinkage at 230 °C as a function of D_{50} for a filling degree of 30 vol.-% and a blend degree of 10 vol.-% of the PP. The unblended compound is added for comparing purposes. The highlighted part refers to the filler type E, and the non-highlighted part to the A glass-type. The blue lines represent the standard deviation of the shrinkage at 230 °C for unfilled PP.

4.2.2 DSC analysis

The DSC test condition is replicated as done in section 3.2.4 and is depicted in Figure 21 for all blended compounds.

Figure 21a and Figure 21b exhibits varying trends in the crystallization temperature depending on the blend type used. For all filler sizes, the addition of am.PA leads to a decrease in the crystallization temperature (roughly 1-2 °C). According to Aranburu and Eguiazabal [4], a slight increase in the crystallization temperature of PP+am.PA blends during cooling was reported, and suggests the slight formation of nucleation site. However quite surprisingly, Aranburu and Eguiazabal [5], also claimed that no change in crystallization temperature was found for PP and am.PA blends after the addition of a filler (organoclay).

The addition of am.PO always leads to an increase in crystallisation temperature (roughly 1-2 °C), regardless of filler type or size (Figure 21a). On the contrary, Ha et al. [22] reported that the recrystallization temperature for a compound of PP and 10 wt.-% am.PO showed a decrease in crystallization temperature.

Forte et al. [1] reported that styrenic based TPE increased the crystallization temperature of PP+TPE blends, and therefore suggests that the styrenic based elastomer acts as nucleation agents for the PP crystals. As can be seen in Figure 21a, TPE added to the compounds revealed similar crystallization temperature trends. For the compounds A-C5.6-30_TPE (PP + comp.+ 10 vol. -% TPE + 30 vol. -% coated A-glass with a D_{50} of 5.6 μm) the crystallization temperature has significantly increased (121.21 ± 0.5 °C) compared to the respective unblended compound (118.71 ± 0.12 °C). However, one exception was observed for A-C31-30_TPE (PP + comp.+ 10 vol. -% TPE + 30 vol. -% coated A-glass with a D_{50} of 31 μm), the decline in crystallization temperature (113.91 ± 0.07 °C) was in line with unfilled PP (113.39 ± 1.1 °C). This phenomenon may be attributed to the formation of more amorphous regions during cooling.

In addition, the same trend towards increasing crystallization temperatures for smaller fillers as described for the unblended compounds can be observed, as the smaller sized fillers can act as nucleating sites [79].

A decline in crystallinity of roughly 4-5 °C, independent on the blend type was observed (Figure 21b). This can be attributed to the increase of amorphous phase in the polymer matrix due to the added amorphous polymer. The major reduction in crystallinity (ca. 17 %) compared to the unblended compound was observed for A-C31-30_TPE (PP + comp.+ 10 vol. -% TPE + 30 vol. -% coated A-glass with a D_{50} of 31 µm) (34.64 ± 0.85 %). However, no dependency of the filler size on the degree of the crystallinity could be found, as all compounds lie within the range of ± 2 %. These small deviations could be referred to slight differences in the sample preparation of the DSC specimens, or could also be within the tolerance of error margin of the DSC machine.

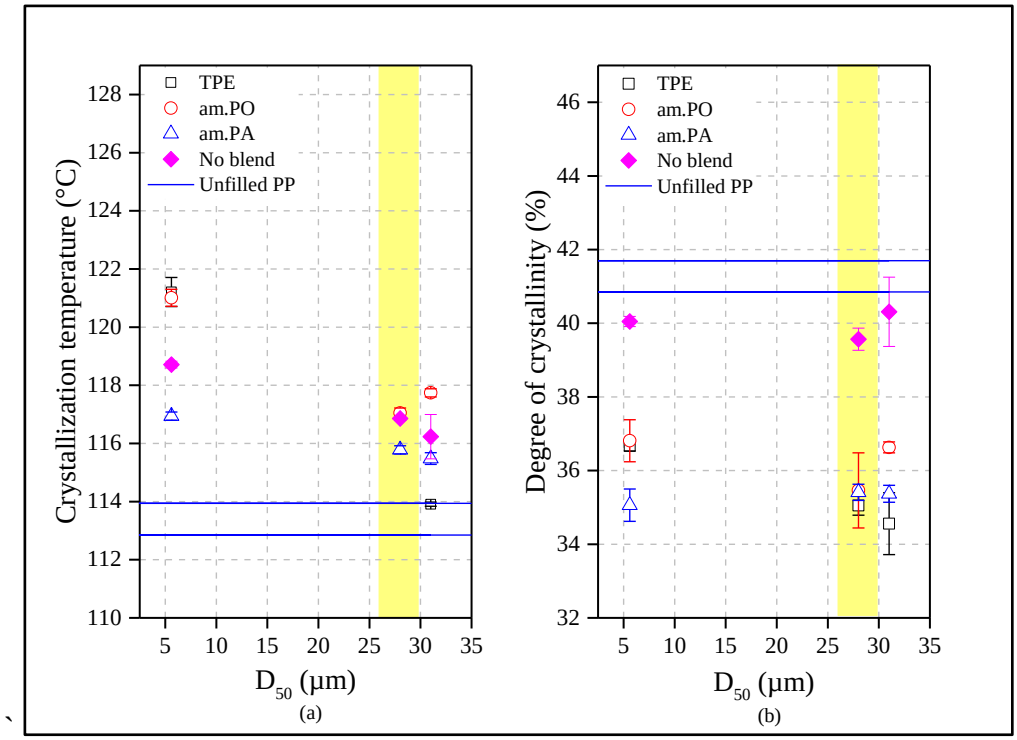

Figure 21: Mean and standard deviation of the crystallization temperature (a) and the degree of crystallinity (b) as a function of D_{50} for a filling degree of 30 vol.-% and a blend degree of 10 vol.-% of the PP. The unblended compound is added for comparing purposes. The highlighted part refers to the filler type E, and the non-highlighted part to the A glass-type. The blue lines represent the standard deviation of the unfilled PP.

4.2.3 Rheology

In this chapter the influence of amorphous polymers on the rheological behaviour of the PP-compounds is discussed Figure 22, Figure 23 and Figure 24 represent the viscosity curves of compounds filled with 30 vol.-% of various sized GB and 10 vol.-% of different blends.

In Figure 22 the viscosity curves for the biggest A-glass type (D_{50} = 31 µm) is depicted as a function of blend types. As the am.PA clearly has the highest viscosity of the added polymers, the compound with am.PA also shows the highest overall viscosity, due to dilution effects. Since the base materials TPE and am.PO obtain a very similar viscosity, also the compound's viscosity is in a similar, but still significantly different, range.

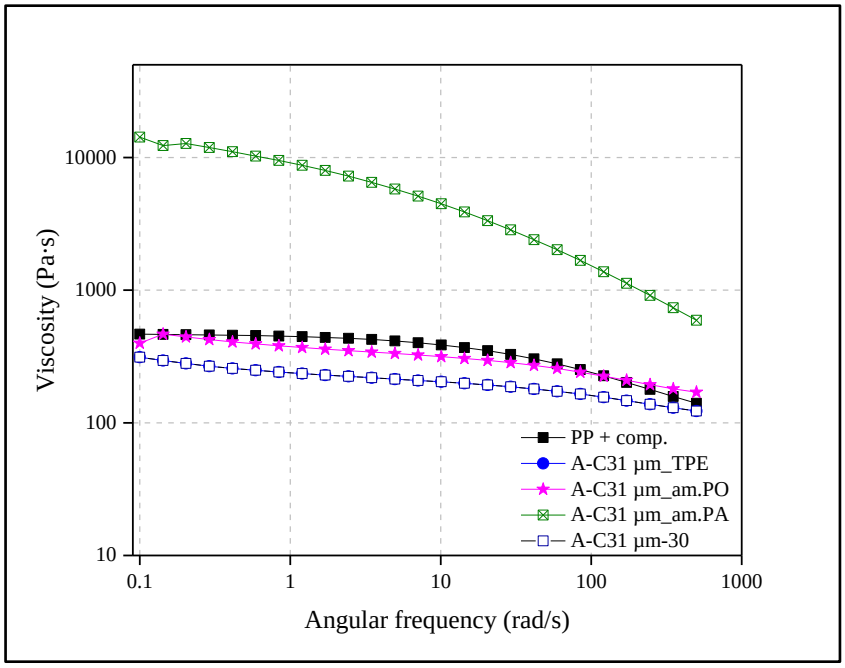

Figure 22: Viscosity as a function of angular frequency for the base compounds and all compounds filled with 30 vol.-% of A-C31 µm with different blend material.

However,in Figure 23 and Figure 24 contradicting results were observed. All blended compounds revealed a viscosity that is increased compared to PP+comp., whereas in Figure 22 the viscosities were partly smaller than that of PP+comp. Moreover, the difference between the addition of TPE and am.PO shows bigger differences, and in Figure 23 even a reversed trend. Without further morphological results, this trend cannot be perfectly described. Furthermore, the addition of blends to the compounds in and leads to a clear reduction of the agglomerations, since no drastic increase in viscosity can be observed for low angular frequencies.

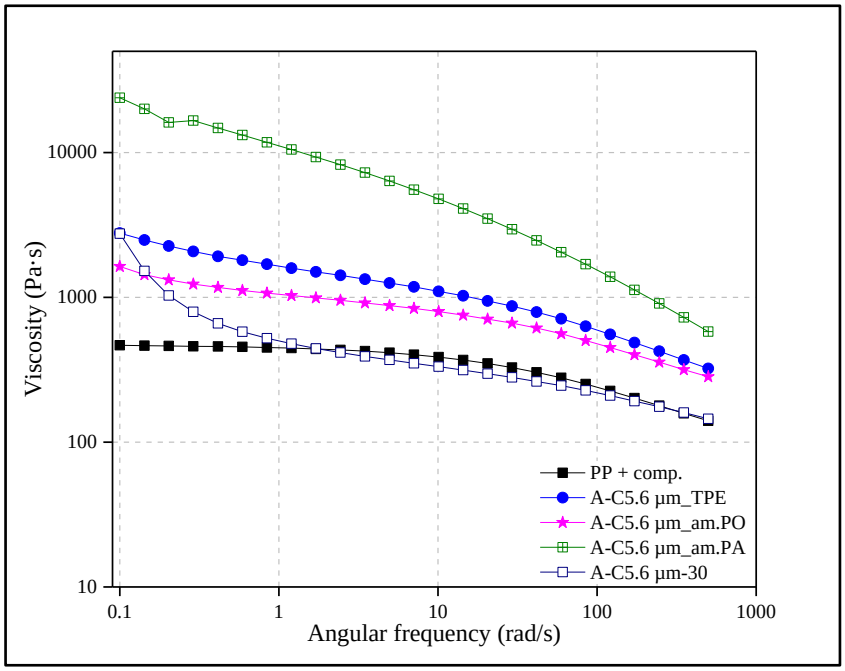

Figure 23: Viscosity as a function of angular frequency for for the base compounds and all compounds filled with 30 vol.-% of A-C5.6 µm with different blend material.

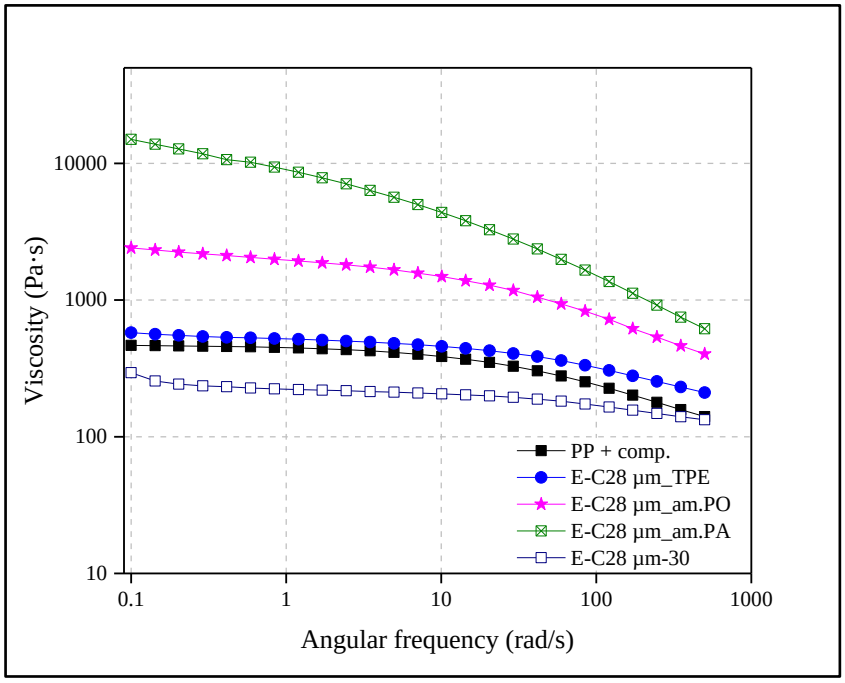

Figure 24: Viscosity as a function of angular frequency for the base compounds and all compounds filled with 30 vol.-% of E-C28 µm with different blend material.

To sum up, the increase in viscosity due to the addition of the blends is for TPE and am.PO not a problem, as their viscosities are well below 1000 Pa·s at 100 1/s [64]. However, the

addition of am.PA showed higher viscosity for all the selected compounds at 100 1/s, making it undesirable for filament printing.

4.2.4 Tensile testing

In Figure 25 the filament elongation at yield (a) and the filament yield stress (b) as a function of filler size is plotted.

For all filler sizes the addition of polymers, independent on their type, leads to an enhancement in filament elongation at yield (Figure 25a) compared to that of the unblended compounds. This can be referred to the reduction of the degree of crystallinity (Figure 21b) [4] or to the relaxations of stress concentrations [22]. The trend of the E-glass type is similar to the results of the unblended compounds, indicating that the interaction between E-glass and polymer is more prominent than between A-glass and PP.

In Figure 25b it can be seen that the blends change the yield stress of the compounds quite drastically (variation between 7 and 21 MPa), whereas no clear trend can be observed. For nearly all compositions, the addition of a blend reduces the yield stress, as already observed by Fasce et al. [13] A similar trend was investigated by Ajili et al. [2] for PP+TPU (50:50) composites, who reported a decrease in yield stress of up to 40 % due to the addition of TPU to PP.

The influence of am.PO and TPE is more pronounced in the A-glass type with 5.6 µm filler than that of 31 µm. The trend for the E-glass type is explained in chapter 4.2.5 by means of SEM analysis. Without SEM micrographs for all other formulations, it is difficult to explain the observed in tensile properties.

As the E-glass type shows the best combination of high yield stress and high filament elongation at yield, the compound E-C28-30_am.PO (PP + comp. + 10 vol. -% am.PO + 30 vol. -% coated E-glass with a D_{50} of 28 µm) was chosen for the extrusion and printing trials.

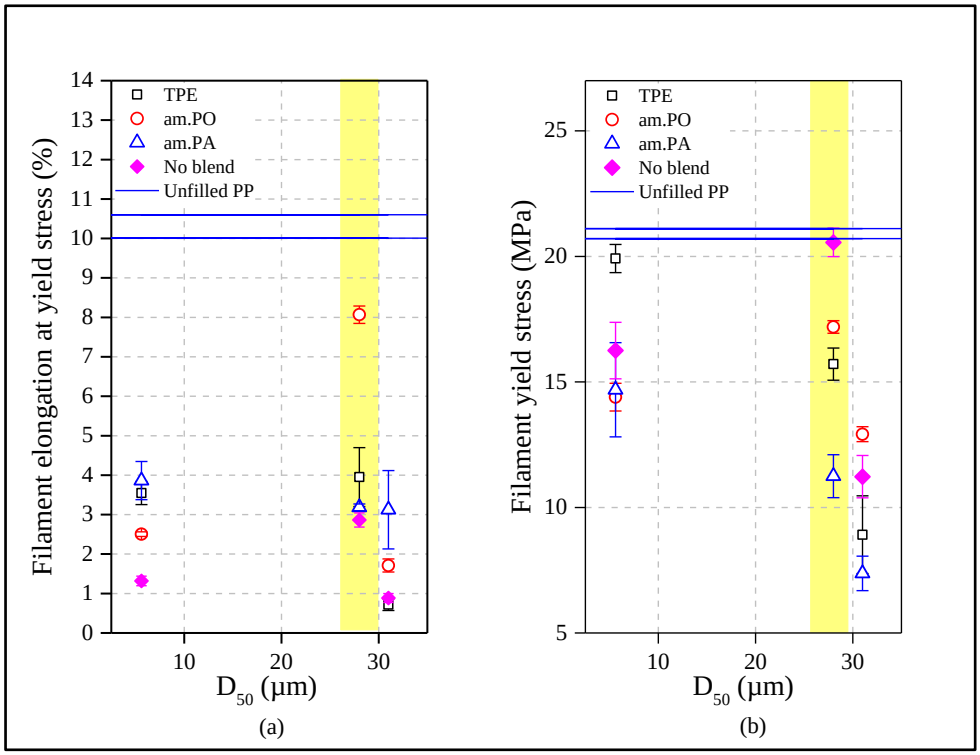

Figure 25: Mean and standard deviation of the filament elongation at yield (a) and the filament yield stress (b) as a function of D50 for a filling degree of 30 vol.-% and a blend degree of 10 vol.-% of the PP. The unblended compound is added for comparing purposes. The highlighted part refers to the filler type E, and the non-highlighted part to the A glass-type. The blue lines represent the standard deviation of the crystallization temperature for unfilled PP.

4.2.5 SEM analysis

In order to study the morphology of coated E-C28-30_am.PO (PP + comp. + 10 vol. -% am.PO + 30 vol. -% coated E-glass with a D_{50} of 28 µm), a cryo-fractured filament was investigated by means of SEM (Figure 26). Both micrographs were captured in different locations of the fracture surface with the same magnification.

In both micrographs (Figure 26) the strong interface between the filler and matrix can be observed, which perfectly reflects the mechanical properties (Figure 25). On both images, the matrix clearly adheres to the filler surface and an even distribution of GB in the polymer matrix can be seen. Contrary to Figure 18, no voids are visible on the fracture surface. Moreover, it is evident that finer fillers are filling the gaps between larger GBs, which is

highly beneficial for mechanical properties and also assists in reducing warpage during filament printing.

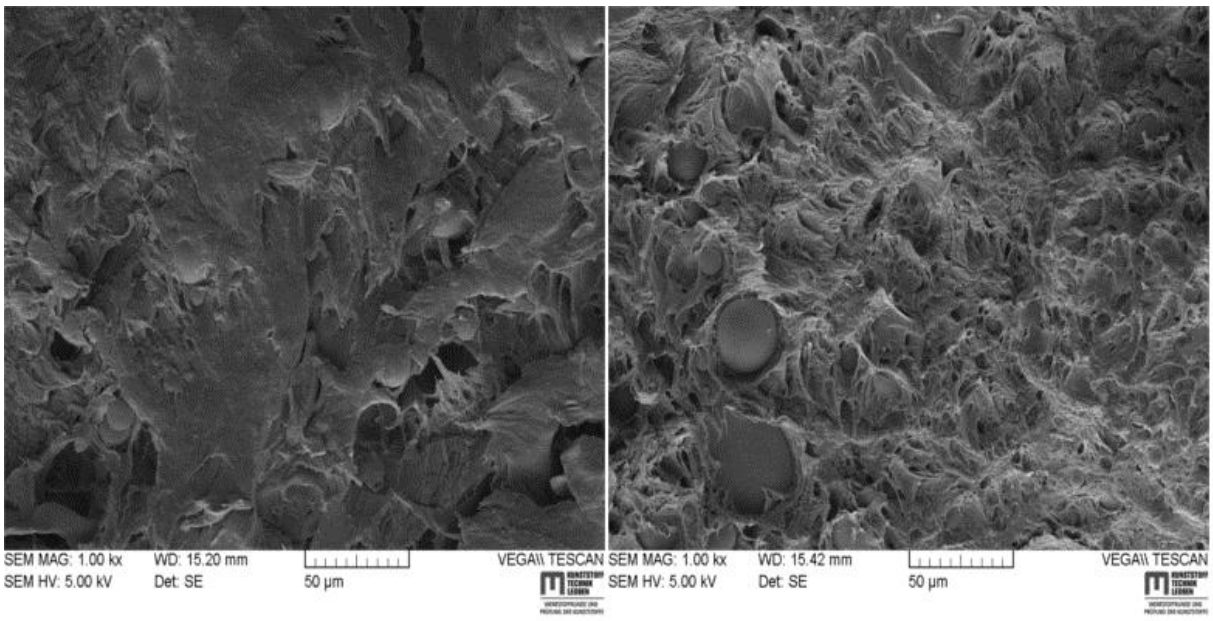

Figure 26: SEM micrographs of two different locations on the facture surface of the compound E-C28-30_am.PO (PP + comp. + 10 vol. -% am.PO + 30 vol. -% coated E-glass with a D_{50} of 28 µm) with the magnifications of 1000x.

4.3 Printing and warpage analysis

Figure 27 shows the warpage results of the compound E-C28-30_am.PO (PP + comp. + 10 vol. -% am.PO + 30 vol. -% coated E-glass with a D_{50} of 28 µm) (a) and the unfilled PP (b). The warpage is indicated by a scale from -1.5 to 2.0 mm, which defines how well the printed part can be compared to the CAD geometry. The green area represents 0 mm in distance to the CAD geometry, which reflects no warpage at all. The blue scale reflects a negative warpage in Z-direction, whereas the red scale represents positive warpage in Z-direction. The histogram next to the scale describes the intensity distribution of the distances to the CAD geometry.

In Figure 27a, the large concentration of the sample part is in the green area, and also the histogram has its maximum number of variables at a distance of 0 mm. Due to the appearance of blue areas, the part tends to warp slightly towards the negative z-direction. In addition, it was expected from the material to warp the most on the edges of the printed product, but the histogram reveals low amount of measured points in that area.

The fact that the printed samples tend to warp non-uniformly in the edge may be attributed to the bed material. As the printing bed material (PP-plate) cannot be perfectly even, the printed first layer may adheres differently over the bed surface. Hence, some edges may adhere to even side of the bed and other edge may tend to warp. This could also be a major cause in distortion observed during printing trials.

On the other hand, the intensity distribution of the unfilled PP (Figure 27b) is skewed towards -0.6 mm, resulting in shrinkage in negative z-direction. Additionally, only small data is recorded at distances values of 0.0 mm and even more points exhibit a higher amount of warpage on two corners. Consequently, E-C28-30_am.PO (PP + comp. + 10 vol. -% am.PO + 30 vol. -% coated E-glass with a D_{50} of 28 µm) blend showed improved shrinkage and warpage properties compared to unfilled PP.

The warpage measurements were done only once with the known set conditions from previous in-house and literature trials [10]. Hence, the data obtained in the current study is not a final result, but rather a first step for further trials required for establishing the suitable process conditions of 3D-printing polypropylene.

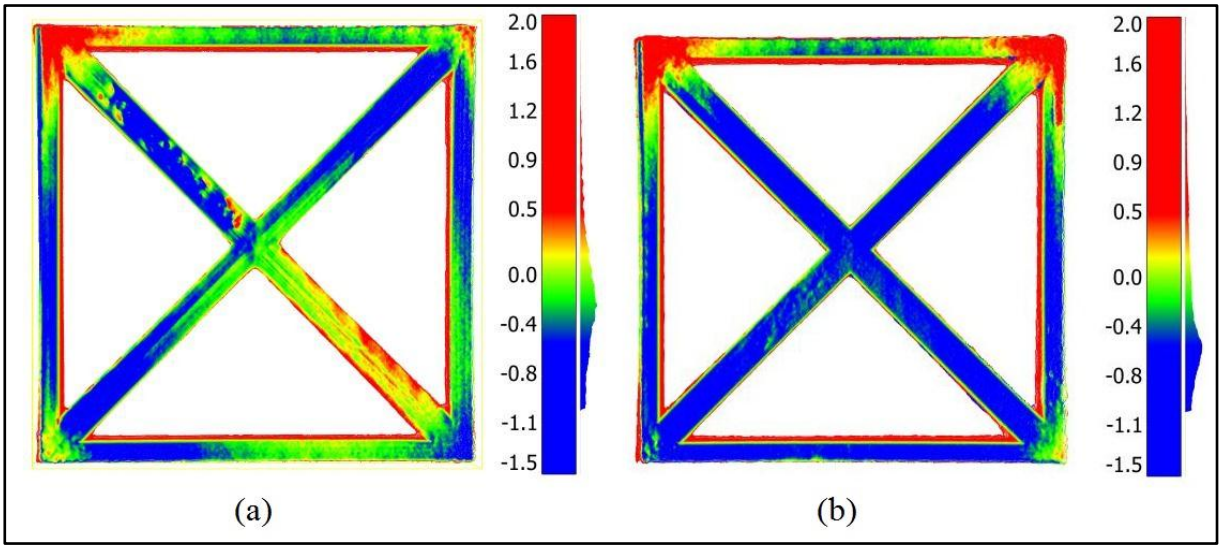

Figure 27: Warpage results of E-C28-30_am.PO (PP + comp. + 10 vol. -% am.PO + 30 vol. -% coated E-glass with a D_{50} of 28 µm) (a) and unfilled PP (b). All the values are the distances to the CAD-file in Z-direction in mm.

5 Summary and conclusion

The main focus of this research work was to improve the printability of PP for the FFF process. To achieve this goal, it was necessary to control and optimize the dimensional stability and warpage of PP. The emphasis was attributed to fill the PP with glass beads of different size and different volume content. In this research two types of GB, the soda lime glass (A-type) and borosilicate glass (E-type), respectively, were selected. The D_{50o} of GB varied from smaller to larger sized GB, 5.6 µm, 18.0 µm and 31.0 µm belong to A-glass type and 28.0 µm belongs to E-glass type. Both glass types were surface treated with and without silane coupling agent. Additionally, the GB were compatibilized with PP grafted with maleic acid anhydride (compatibilizer) to enhance the interaction between the filler and matrix. The successful selection of filler system was carried out by formulating 16 initial compounds with varying filler type and volume content.

pvT measurement were carried out to investigate the influence of filler type and volume content. At 15 vol.- % all the 16 formulations showed approximately a reduction of 10 % in shrinkage recorded at 230 °C when measured in comparison to unfilled PP. However, by increasing the filler content to 30 vol.- %, all formulations recorded an average shrinkage reduction of 30 %.

DSC analyses illustrate that the results obtained led to a very small change in crystallinity regardless of filler type and volume content. Moreover, smaller sized GB increased the β-nucleation which resulted in an increase in the crystallization temperature.

The rheology results revealed that all compounds lie well beneath the minimal requirement of 1000 Pa·s at 100 1/s for filament printing except for compounds blend with am.PA.

The minimal requirement for filaments to print is to have high stiffness, yield stress and elongation at yield, so as to avoid the buckling of the filament during printing. The most promising compounds revealed similar yield stress values as unfilled PP, but a drastic decrease in elongation at yield due to the high filling degree. The main difference in terms of coating influence had shown that with coating the filament tensile properties were better than that of uncoated fillers of respective sizes. The mechanical properties were also validated by means of scanning electron microscopy.

In order to enhance the elongation at yield, three different polymer types (TPE, am.PO, am.PA) were added to the three most promising compounds. No influence of the blend type was observed for the shrinkage values and the degree of crystallization, whereas the crystallization temperature further increased. The rheological behaviour showed only a slight increase in viscosity for am.PO and TPE, whereas am.PA led to too high viscosity values.

The best enhancement of the elongation at yield was achieved by the addition of am.PO. Hence, one compound consisting of PP, compatibilizer, 30 vol.-% of coated borosilicate glass with a D_{50} of 28 µm and 10 vol.-% of am.PO was chosen for filament extrusion and subsequent printing trials.

After successful extrusion of the filaments and 3D-printing of parts, the printed samples were compared to unfilled PP. Eventually, the warpage results were clearly improved and will set forth basis for future printing trials.

As the smaller sized fillers effected the compounds with overall better properties, tremendous potential for further investigation would lie in the use of very small sized E-glass fillers. The future potential in the field of 3D printing lies in developing novel materials for design and process specific applications. With a few more trials in printing and mechanical characterization we can surely add one more potential material viable for 3D printers.

6 References

[1] Abreu F.O.M.S., Forte M.M.C., Liberman S.A.: SBS and SEBS block copolymers as impact modifiers for polypropylene compounds, Journal of Applied Polymer Science 95 (2), 2005, S. 254–263

[2] Ajili S.H., Ebrahimi N.G., Khorasani M.T.: Study on thermoplastic polyurethane/polypropylene (TPU/PP) blend as a blood bag material, Journal of Applied Polymer Science 89 (9), 2003, S. 2496–2501

[3] Annicchiarico D., Alcock J.R.: Review of Factors that Affect Shrinkage of Molded Part in Injection Molding, Materials and Manufacturing Processes 29 (6), 2014, S. 662–682

[4] Aranburu N., Eguiazabal J.I.: Compatible blends of polypropylene with an amorphous polyamide, Journal of Applied Polymer Science 127 (6), 2013, S. 5007–5013

[5] Aranburu N., Eguiazábal J.I.: Organoclay-reinforced compatible blends of polypropylene with an amorphous polyamide, Polymer Engineering & Science 54 (12), 2014, S. 2762–2769

[6] Bai S.-L., Chen J., Huang Z., Yu Z.: The role of the interfacial strength in glass bead filled HDPE, Journal of Materials Science Letters 19 (17), 2000, S. 1587–1589

[7] Balkan O., Ezdeşir A.: Rheological behaviors of glass bead- and wollastonite-filled polypropylene composites modified with thermoplastic elastomers, Polymer Composites 33 (7), 2012, S. 1162–1187

[8] Bicerano J.: Prediction of Polymers Properties, Third Edition, Revised and Expanded, 3. Ed., MARCEL DEKKER, INC, New York, 2002

[9] Brown R.: Handbook of Polymer Testing: Short-term Mechanical Tests, Rapra Technology Limited, Shawbury, UK, 2002

[10] Carneiro O.S., Silva A.F., Gomes R.: Fused deposition modeling with polypropylene, Materials & Design 83, 2015, S. 768–776

[11] Christ S., Schnabel M., Vorndran E., Groll J., Gbureck U.: Fiber reinforcement during 3D printing, Materials Letters 139, 2015, S. 165–168

[12] Dul S., Fambri L., Pegoretti A.: Fused deposition modelling with ABS–graphene nanocomposites, Composites Part A: Applied Science and Manufacturing 85, 2016, S. 181–191

[13] Fasce L.A., Pettarin V., Marano C., Rink M., Frontini P.M.: Biaxial yielding of polypropylene/elastomeric polyolefin blends, Effect of elastomer content and thermal annealing, Polymer Engineering & Science 48 (7), 2008, S. 1414–1423

[14] Faulkner D.L., Schmidt L.R.: Glass bead-filled polypropylene part I, Rheological and mechanical properties, Polymer Engineering and Science 17 (9), 1977, S. 657–665

[15] Fischer J.M.: Handbook of molded part shrinkage and warpage, PDL handbook series, Elsevier, Amsterdam, 2013

[16] Fu S.-Y., Feng X.-Q., Lauke B., Mai Y.-W.: Effects of particle size, particle/matrix interface adhesion and particle loading on mechanical properties of particulate–polymer composites, Composites Part B: Engineering 39 (6), 2008, S. 933–961

[17] Gardner D.J., Han Y., Wang L.: Wood–Plastic Composite Technology, Current Forestry Reports 1 (3), 2015, S. 139–150

[18] Gebhardt A.: Rapid Prototyping, 1. Ed., Hanser Gardener Publications, Munich, 2003

[19] Gerard J.-F.: Fillers and filled polymers, Wiley-VCH, Lyon, France, 2001

[20] Grellmann W., Seidler S.: Polymer Testing, 2. Ed., Hanser Publications, 2007

[21] Gurr M., Mülhaupt R.: Rapid Prototyping, In: Moeller M., Matyjaszewski K. (Ed.): Polymer Science, A Comprehensive Reference,, Elsevier, Amsterdam, 2012, S. 77–99

[22] Ha H.S., Woo J.Y., Kim W.H., Kim H.S., Kim B.K.: The rheological, thermal, and mechanical properties for polypropylene and amorphous poly alpha olefin blends, Polymers for Advanced Technologies 19 (1), 2008, S. 47–53

[23] Harper C.A.: Modern plastics handbook, McGraw-Hill, New York, 2000

[24] Hui Z., Yuan Z.H., Long Z.Y., Wen W.Q.: Research of Wood Plastic Composites application based on Fused Deposition Modeling technology, In: Mechanical Engineering and Information Technology (EMEIT), 2011, S. 1560–1562

[25] Ibrahim M., Badrishah N.S., Sa'ude N., Ibrahim M.H.I.: Sustainable Natural Bio Composite for FDM Feedstocks, Applied Mechanics and Materials 607, 2014, S. 65–69

[26] Kalita S.J., Bose S., Hosick H.L., Bandyopadhyay A.: Development of controlled porosity polymer-ceramic composite scaffolds via fused deposition modeling, Materials Science and Engineering: C 23 (5), 2003, S. 611–620

[27] Kannan M., Bhagawan S.S., Thomas S., Joseph K.: Nanoclay effect on transport properties of thermoplastic polyurethane/polypropylene (TPU/PP) blends, Journal of Polymer Research 20 (8), 2013

[28] Kannan M., Bhagawan S.S., Thomas S., Joseph K.: Thermogravimetric analysis and differential scanning calorimetric studies on nanoclay-filled TPU/PP blends, Journal of Thermal Analysis and Calorimetry 112 (3), 2013, S. 1231–1244

[29] Karger-Kocsis J.: Polypropylene An A-Z reference, Polymer Science and Technology Series, 0093-6286, Vol. 2, Springer Netherlands; Imprint; Springer, Dordrecht, 1999

[30] Kovács J.G., Solymossy B.: Effect of glass bead content and diameter on shrinkage and warpage of injection-molded PA6, Polymer Engineering & Science 49 (11), 2009, S. 2218–2224

[31] Li R., Liang J.-Z., Tjong S.C.: Morphology and dynamic mechanical properties of glass beads filled low density polyethylene composites, Journal of Materials Processing Technology 79 (1-3), 1998, S. 59–65

[32] Liang J.-Z., Li R., Tang C.Y., Wong T.T.: Tensile yield behaviour of glass bead filled LDPE composites, METALS AND MATERIALS, 4 (3), 1998, S. 256–268

[33] Liang J.-Z., Li R., Tjong S.C.: Effects of pressure and temperature on the melt density and the melt flow rate of LDEP and glass bead-filled LDPE composite, Journal of Materials Processing Technology 91 (1-3), 1999, S. 167–171

[34] Liang J.-Z., Li R., Tjong S.C.: Morphology and tensile properties of glass bead filled low density polyethylene composites, Polymer Testing 16 (6), 1998, S. 529–548

[35] Liang J.-Z., Li R., Tjonga S.C.: Effects of glass bead size and content on the viscoelasticity of filled polypropylene composites Polymer Testing (19), 2000, S. 213–220

[36] Liang J.-Z., Li R.: Brittle–ductile transition in polypropylene filled with glass beads, Polymer 40 (11), 1999, S. 3191–3195

[37] Liang J.Z., Li R.K., Tang C.Y., Cheung S.W.: The Melt Shear Viscosity of Polypropylene/Glass bead Composites at High Extrusion Flow Rates, In: Massard T.E., Vautrin A.E. (Ed.), Twelfth international conference on composite materials, ----------, Quincy MA, 2000

[38] Liang J.-Z.: The melt elastic behavior of polypropylene/glass bead composites in capillary flow, Polymer Testing 21 (8), 2002, S. 927–931

[39] Liu F., Zeng S., Zhou H., Li J.: A Study on the Distinguishing Responses of Shrinkage and Warpage to Processing Conditions in Injection Molding, Journal of Applied Polymer Science 125 (1), 2012, S. 731–744

[40] Makhlouf A., Satha H., Frihi D., Gherib S., Seguela R.: Optimization of the crystallinity of polypropylene/submicronic-talc composites, The role of filler ratio and cooling rate, Express Polymer Letters 10 (3), 2016, S. 237–247

[41] Mallick P.K., Broutman L.J.: Mechanical and fracture behaviour of glass bead filled epoxy composites, Materials Science and Engineering 18 (1), 1975, S. 63–73

[42] Masood S.H., Song W.: Development of new metal/polymer materials for rapid tooling using Fused deposition modelling, Materials & Design 25 (7), 2004, S. 587–594

[43] Mezger T.G.: The Rheology Handbook: For Users of Rotational and Oscillatory Rheometers, Vincentz Network, 2006

[44] Miyazaki K., Hamadate M., Terano M., Nakatani H.: Syndiotactic polypropylene/microfibrous cellulose composites, Effect of filler size on tensile properties, Journal of Applied Polymer Science 128 (1), 2013, S. 915–922

[45] Mohamed O.A., Masood S.H., Bhowmik J.L.: Optimization of fused deposition modeling process parameters, A review of current research and future prospects, Advances in Manufacturing 3 (1), 2015, S. 42–53

[46] Moore P.E.: Polypropylene Handbook, Polymerization, Characterization, Properties, Processing, Applications, Hanser Publications, Cincinnati, 1996

[47] N.N.: Comparative data PC/ABS - Microperl® glass bead vs. glass fibers, http://polymer-additives.specialchem.com/tech-library/technical-paper/comparative-data-microperl-glass-bead-pc-abs-resin/download (Retrieved on: 10.01.2017)

[48] N.N.: Eastman Aerafin™ 180 Polymer | TDS |, Dresden, Germany, 2015, http://www.eastman.com/ (Retrieved on: 09.01.2017)

[49] N.N.: How to get clean surface aspect when using glass beads in PA parts, http://polymer-additives.specialchem.com (Retrieved on: 10.01.2017)

[50] N.N.: PP BD212CF Produkt information, Vienna, 2010, borealisgroup.com (Retrieved on: 03.11.2016)

[51] N.N.: Spheriglass® Technical data sheet 2000 and 3000E, Kirchenheimbolanden, D, www.potterseurope.com (Retrieved on: 10.01.2017)

[52] N.N.: TA INSTRUMENTS DIFFERENTIAL SCANNING CALORIMETER (DSC), TA Q100 DSC Operating Instructions (Retrieved on: 04.11.2016)

[53] N.N.: Technical data sheet Henkel Macromelt PA 6797, Heidelberg, Germany, 2004, www.industrial-adhesives.com (Retrieved on: 27.12.2016)

[54] N.N.: Technical datasheet Kraiburg TPE TF6TAA, Waldkraiburg, Germany, http://www.kraiburg-tpe.com/ (Retrieved on: 09.01.2017)

[55] Nikzad M., Masood S.H., Sbarski I.: Thermo-mechanical properties of a highly filled polymeric composites for Fused Deposition Modeling, Materials & Design 32 (6), 2011, S. 3448–3456

[56] Ning F., Cong W., Qiu J., Wei J., Wang S.: Additive manufacturing of carbon fiber reinforced thermoplastic composites using fused deposition modeling, Composites Part B: Engineering 80, 2015, S. 369–378

[57] Osswald T.A.: Understanding polymer processing, Processes and governing equations, Hanser, München, 2011

[58] Quan Z., Wu A., Keefe M., Qin X., Yu J., Suhr J., Byun J.-H., Kim B.-S., Chou T.-W.: Additive manufacturing of multi-directional preforms for composites, Opportunities and challenges, Materials Today 18 (9), 2015, S. 503–512

[59] R. Nasrin, A. H. Bhuiyan, Md. A. Gafur.: Isotactic polypropylene – talc composites, Mechanical properties, Electrical behavior, International Journal of Composite Materials 5 (6), 2015, S. 155–161

[60] Ramli M.S., Wahab M.S., Ahmad M., Bala A.S.: FDM preparation of bio-compatible UHMWPE polymer for artificial implant, ARPN Journal of Engineering and Applied Sciences 11 (8), 2016

[61] Roberson D.A., Siqueiros J.G.: Novel Polycarbonate/SEBS-g-MA Blend for FDM-Type 3D Printing, In: ANTEC 2016, Proceedings of the technical conference & exhibition, Indianapolise, USA, 2016

[62] Rocha C.R., Torrado Perez A.R., Roberson D.A., Shemelya C.M., MacDonald E., Wicker R.B.: Novel ABS-based binary and ternary polymer blends for material extrusion 3D printing, Journal of Materials Research 29 (17), 2014, S. 1859–1866

[63] Shah V.: Handbook of plastics testing and failure analysis, 3. Ed., Wiley, Chichester, 2007

[64] Spörk M., Gonzalez-Gutierrez J., Kukla C., Schuschnigg S., Holzer C.: Special Materials and Technologies for Fused Filament Fabrication, In: Wang Q. (Ed.), Polymer Processing Society Asia/Australia, China, 2016

[65] Strong A.B.: Plastics, Materials and processing / A. Brent Strong, 3. Ed., Prentice Hall, Englewood Cliffs, N.J., London, 2006

[66] Tang T., Jing X., Huang B.: Studies on compatibilization of polypropylene/thermoplastic polyurethane blends and mechanism of compatibilization, Journal of Macromolecular Science, Part B 33 (3), 1994, S. 287–305

[67] Tekinalp H.L., Kunc V., Velez-Garcia G.M., Duty C.E., Love L.J., Naskar A.K., Blue C.A., Ozcan S.: Highly oriented carbon fiber–polymer composites via additive manufacturing, Composites Science and Technology 105, 2014, S. 144–150

[68] Tolinski M.: Additives for polyolefins, Getting the most out of polypropylene, polyethylene and TPO, PDL handbook series, 1. Ed., William Andrew Publishing, Oxford, 2009

[69] van Krevelen D.W., te Nijenhuis K.: Properties of Polymers: Their Correlation with Chemical Structure; their Numerical Estimation and Prediction from Additive Group Contributions, Elsevier Science, 2009

[70] Vidović E., Faraguna F., Jukić A.: Influence of inorganic fillers on PLA crystallinity and thermal properties, Journal of Thermal Analysis and Calorimetry, 2016

[71] Volpato N., Kretschek D., Foggiatto J.A., Gomez da Silva Cruz C.M.: Experimental analysis of an extrusion system for additive manufacturing based on polymer pellets, The International Journal of Advanced Manufacturing Technology 81 (9-12), 2015, S. 1519–1531

[72] Wang J.: pvT Properties of Polymers for Injection Molding, Some Critical Issues for Injection Molding, 2005, http://www.intechopen.com (Retrieved on: 04.11.2016)

[73] Weng Z., Wang J., Senthil T., Wu L.: Mechanical and thermal properties of ABS/montmorillonite nanocomposites for fused deposition modeling 3D printing, Materials & Design 102, 2016, S. 276–283

[74] White J.L., Choi D.D.: Polyolefins, Processing, structure development and properties, Hanser Gardner Publications, Cincinnati, 2005

[75] Wypych G.: Handbook of fillers, Elsevier Science, 2016

[76] Yang W., Liu Z.-Y., Shan G.-F., Li Z.-M., Xie B.-H., Yang M.-B.: Study on the melt flow behavior of glass bead filled polypropylene, Polymer Testing 24 (4), 2005, S. 490–497

[77] Yang W., Shi W., Li Z.-M., Xie B.-H., Feng J.-M., Yang M.-B.: Mechanical Properties of Glass Bead-Filled Linear Low-Density Polyethylene, Journal of Elastomers and Plastics 36 (3), 2004, S. 251–265

[78] Yuan Q., Jiang W., An L., Li R., Jiang Z.: Mechanical and thermal properties of high-density polyethylene toughened with glass beads, Journal of Applied Polymer Science 89 (8), 2003, S. 2102–2107

[79] Yuan Q., Jiang W., An L., Misra R.: Effects of reinforcement filler and temperature on the stability of β-crystal in glass bead filled polypropylene, Materials Science and Engineering: A 415 (1-2), 2006, S. 297–303

[80] Yuan Q., Jiang W., Zhang H., Yin J., An L., Li R.: Brittle-ductile transition in high-density polyethylene/glass-bead blends: Effects of interparticle distance and temperature, Part B: Polymer Physics, Journal of Applied Polymer Science 39, 2001, S. 1855–1859

[81] Zhong W., Li F., Zhang Z., Song L., Li Z.: Short fiber reinforced composites for fused deposition modeling, Materials Science and Engineering: A 301 (2), 2001, S. 125–130

7 List of Figures and Tables

8 List of Abbreviations and acronyms

PP	Polypropylene
Comp.	Compatibilizer
FFF	fused filament fabrication
TPE	thermoplastic elastomers
am.PA	amorphous polyamides
am.PO	amorphous polyolefin
FDM	Fused deposition modelling
SEM	Scanning electron microscopy
CAD	Computer Aided Drawing
GB	Glass bead
DSC	Differential scanning calorimeter
UHMW-PE	ultra-high molecular weight polyethylene,
MFR	melt flow rate
HDPE	High density polyethylene
Type E	Borosilicate glass beads
Type A	Lime-soda glass beads
C and UC	coated and uncoated respectively
CP03	suppliers code name for silane coupling agent
UTM	universal testing machine
kN,	kilo Newton
MPa,	Mega Pascal
Pa·s	Pascal second
pvT,	Pressure-Volume-Temperature